Modelling the tides of the southern Weddell Sea

Thesis

UNRESTRICTED

MODELLING THE TIDES OF THE SOUTHERN WEDDELL SEA

ALLAN ROBINSON

A thesis submitted in partial fulfilment of the
requirements of the Open University
for the degree of Master of Philosophy

February 1996

British Antarctic Survey in collaboration with
Proudman Oceanographic Laboratory

Date of submission: February 1996
Date of award: October 1996

ProQuest LLC.
789 East Eisenhower Parkway
P.O. Box 1346
Ann Arbor, MI 48106 – 1346

Modelling the tides of the southern Weddell Sea

Allan Robinson

February 1996

Abstract

Numerical modelling presented in this thesis reproduces the tides of the Weddell Sea, a region where a significant proportion of a globally important water mass, Antarctic Bottom Water is generated. The presence of the Filchner and Ronne Ice Shelves in the southern Weddell Sea, and heavy pack ice conditions in the rest of the Weddell Sea have greatly restricted direct observations of the general oceanography. By producing tidal maps for the whole of the Weddell Sea which are in agreement with the available data, this study has contributed to the understanding of the general oceanography of this important region. In addition, the following conclusions can also be drawn. The presence of the ice shelves in the southern Weddell Sea has little effect upon the tides except for the reduction in water column thickness. This means that the value of the friction coefficient at the ice-ocean interface is no more important than the value of the friction coefficient at the sea floor. Ice shelf flexure at grounding lines has a significant but highly localised effect upon the tides, the effect not being seen at sites some distance from grounding lines. This suggests that ice shelf flexure is not a significant mechanism for tidal energy dissipation. The results from the tidal model were affected by changes to the water column, but indicated that given the correct bathymetry the model would produce accurate results. The model results also suggested that the most significant areas of tidal energy dissipation are the shallowest areas of the continental shelf. Because of the effect of the ice shelf on reducing the water column thickness this locates these areas on the continental shelf just "inshore" from the front of the Ronne Ice Shelf, though the continental shelf break was also significant.

ACKNOWLEDGEMENTS

My supervisors have given me invaluable help throughout this project, and so in brief I would like to thank Dr. Chris Doake for his support and inspiration, Dr. Mike Smithson for introducing me to tidal modelling, and last but not least Dr. Keith Nicholls for extensive help and guidance throughout my career at the British Antarctic Survey.

Special thanks are also due to Dr. Roger Flather who provided the tidal model which was used for this project.

I would also like to thank David Vaughan who provided the datasets for Filchner-Ronne Ice Shelf and converted the model results into the form required for the ESAMCA programme, and Keith Makinson for asking penetrating questions and putting up with sharing an office with me.

Finally, I would like to thank my wife, Kay, whose patience, care and support through hard disk failures and printer problems made this thesis possible.

TABLE OF CONTENTS:

LIST OF FIGURES:

LIST OF TABLES:

LIST OF ACRONYMS:

AABW	Atlantic Antarctic Bottom Water
WSBW	Weddell Sea Bottom Water
WDW	Warm Deep Water
MWDW	Modified Warm Deep Water
WSW	Western Shelf Water
ESW	Eastern Shelf Water
WW	Winter Water
ISW	Ice Shelf Water
ESAMCA	Exploitation of Satellite Altimetry for Monitoring Climate change in Antarctic ice shelves.
SCH	Schwiderski (1980) open boundary condition data.
CR	Cartwright and Ray (1990) open boundary condition data.
O1	Principal lunar diurnal tide
K1	Principal lunar/solar diurnal tide
M2	Principal lunar semi-diurnal tide
S2	Principal solar semi-diural tide

Chapter 1:

Why model the tides of the Weddell Sea.

The Weddell Sea is a region of global oceanographic importance. The majority of Antarctic Bottom Water (hereafter ABW), a water mass found in deep oceans as far as 50° N (Dietrich, 1980; Mantyla & Reid, 1983) is formed in the Weddell Sea (Foldvik and Gammelsrød, 1988; Deacon, 1937). The presence of Filchner-Ronne Ice Shelf in the southern part of the Weddell Sea (Figure 1.1) both contributes to the production of ABW (Foldvik and Gammelsrød, 1988) and makes data collection difficult. Most work has been confined to cruises along the ice front of the ice shelves (Foldvik et al, 1985a, 1985b; Seabrooke et al, 1971) where a shore lead often exists, and to work in the central part of the Weddell Sea (Fahrbach, 1994b; Gill, 1973; Foster and Carmack, 1976). In addition, oceanographic profiling has been carried out via two holes drilled through the Ronne Ice Shelf (Nicholls et al, 1991, Nicholls & Jenkins, 1993; Robinson et al, 1994), and deductions about the pattern of ocean currents under the ice shelf have been made using geophysical techniques (Robin et al, 1983). All together this work has demonstrated that ABW can be formed by two different processes.

One process is frontal zone mixing (Foster et al, 1987; Foster and Carmack, 1976) between modified Warm Deep Water from the deep ocean basin and Western Shelf Water (a water mass formed by brine rejection during the

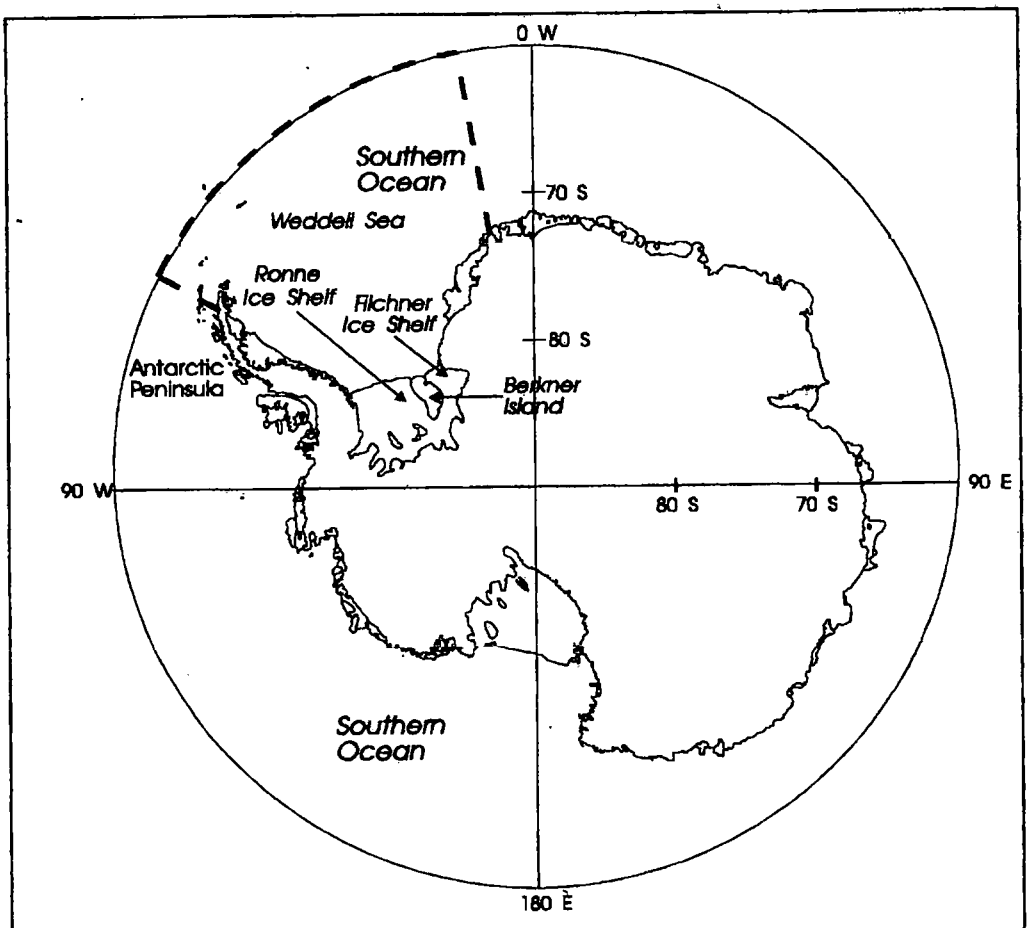

Figure 1.1: *Map of Antarctica showing location of Weddell Sea in relation to the rest of Antarctica. The positions of Filchner Ice Shelf, Ronne Ice Shelf and Berkner Island are indicated. Model open boundaries are shown by heavy dashed lines.*

formation of sea-ice, hereafter WSW). The dense product of this mixing is Weddell Sea Bottom Water (hereafter WSBW) which forms the deepest layer of water in the Weddell Sea, and is modified during its passage out of the Weddell Sea basin to form ABW (see Figure 1.2 for relative characteristics of the water masses found in the Weddell Sea).

Another process involves Ice Shelf Water (hereafter ISW), a dense water mass with a temperature lower than the surface freezing point which is produced in the sub-ice shelf cavity by melting of the ice shelf from contact between the ice shelf and WSW. Plumes of ISW have been observed flowing out over the

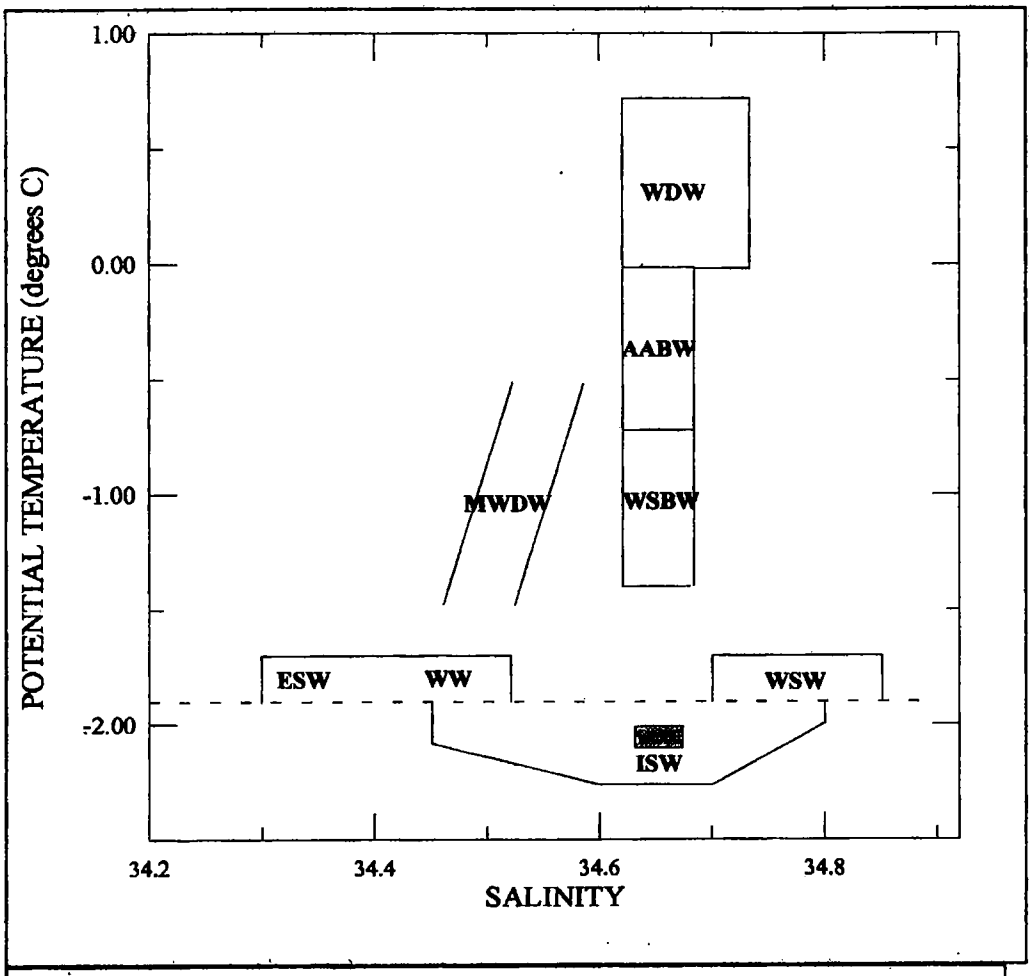

Figure 1.2: *Schematic representation of the different water masses found in the Weddell Sea. The broken line represents the surface freezing point. The shaded rectangle represents the characteristics of ISW that flows over the continental shelf break into the central Weddell Sea*

continental shelf and down the continental slope, where ISW mixes with Warm Deep Water (hereafter WDW) to form WSBW.

Tides will play an important role in both processes by generating mixing between the different water masses. Tidal currents assist the formation of WSW by maintaining the lead in the sea-ice that is adjacent to the front of the ice shelves (Foldvik and Gammelsrød, 1988). Beneath the ice shelf tidal motion will also be an important mechanism for the mixing and transport of water masses, because of the isolation of this environment from the effects of wind.

Unfortunately the lack of tidal data in the region (and in the Southern Ocean in general) mean that the tides are not known to any great accuracy. In addition the presence of sea-ice in the Weddell Sea renders satellite altimetry useless, while the poorly known geoid and atmospheric corrections make measurements over the Filchner-Ronne Ice Shelf highly erroneous, thus preventing the use of satellite altimetry for direct observation of tidal motions, as has been done in other parts of the global ocean (e.g. Cartwright and Ray, 1990). Therefore the only currently available method of gaining information on the tides is to model them.

The project has two driving motivations: the first is to provide a dataset which can be used to calculate a tidal correction for ERS-1 satellite altimeter heights, as part of the ESAMCA programme to enable very accurate measurements of the altitude of the ice shelf surface; the second is to gain a better picture of how the tides affect the general oceanography of the area. Both will require achieving as good a fit as is possible with what is known about the tides, as well as an understanding of where the model may be falling down.

Previous work on modelling the tides on Antarctic ice shelves is limited to two examples:
MacAyeal (1979) applied a finite-diference model of the tides to the Ross Ice Shelf and the adjacent continental shelf, with the aim of studying controls on the glaciological regime of the ice shelf, through the effect of tides upon the sub-ice shelf oceanography (MacAyeal, 1984a, 1984b). This model used a spatially regular grid and a time-stepping procedure to integrate the hydrodynamic equations forward through time. The six largest tidal constituents (O1, P1, K1, N2, M2, S2) were used in the model and each tidal constituent was treated separately, thus preventing interactions between the different constituents. This model did not acheive satisfactory agreement between the observed and simulated semi-diurnal constituents.

Le Provost and Vincent (1986) developed a finite-element tidal model using the 8 largest tidal constituents (M2, S2, N2, K2, 2N2, K1, O1, Q1) which has been used to produce maps of the K1 and M2 tidal constituents in the South Atlantic Ocean (Genco et al, 1994), in addition to being applied to the global ocean (Le Provost et al, 1994). This model used an irregular grid which provided a greater density of grid points to be used where required. The form of solution of the hydrodynamic equations used was such that the velocity field associated with each tidal constituent was a derivative of the sea surface elevation. At present this method of producing velocities requires further calibration to achieve accurate results (Genco et al, 1994). This model has achieved very good agreement between the observed and simulated tidal amplitudes and phases for the M2 and K1 constituents.

Both models were driven by a combination of the equilibrium tide and specified tidal motion along the open boundary of the model, taken from a global ocean tidal model, and were compared with available in situ data.

The Proudman Oceanographic Laboratory had developed a "Tide + Storm Surge" model (hereafter called the Flather model) which is used by the U.K. Meteorological Office in operational prediction of storm surges in the North Sea (Proctor and Flather, 1983) and around the coast of Britain. This model is depth-averaged (two-dimensional), has been applied to several different areas (Flather, 1994, 1988, 1987), and has been used to provide boundary conditions for regional tidal models (Gjevik et al, 1994). Because the performance of the model is well known, it is an ideal model to apply to a previously unmodelled area, the Weddell Sea. It can be driven with up to 15 tidal constituents, and tidal currents are a direct product of the model. Thus it has advantages over the MacAyeal (1979) model because interactions between different tidal constituents are possible, and over the Genco et al (1994) model because of the calculation of tidal currents within the model.

In the next chapter I will describe the Flather model, the modifications that were made to the model to apply it to the Weddell Sea and the model domain with which it will be used.

Chapter 2:

The tidal model.

INTRODUCTION

In this chapter I will briefly describe the numerical model that was used, covering the constituent equations upon which it is based, the structure of the computer programs which compose the model, and the data sets from which were derived the model boundary conditions and domain. The structure of the model is relevant to this discussion because of the effect it has on efforts to modify the standard tidal model to take account of the unusual environment found in the southern Weddell Sea. Knowledge of the quality of open boundary condition and model domain data sets will provide information about the expected accuracy of the modelled tides.

THE NUMERICAL MODEL OF TIDES

The model is fully described in Flather (1994) so only a basic description will be given here. The constituent equations upon which the model is based are the equation of continuity (conservation of volume) in its depth-averaged, spherical polar co-ordinates form:

$$\frac{\partial \zeta_s}{\partial t} + \frac{1}{R\cos}\frac{\partial}{\partial \chi}(Du) + \frac{\partial}{\partial \phi}(Dv\cos) = 0 \qquad (1)$$

and the Navier-Stokes equations which relate the balance of horizontal accelerations:

$$\frac{\partial u}{\partial t}+\frac{u}{R\cos\varphi}\frac{\partial u}{\partial \chi}+\frac{v}{R}\frac{\partial u}{\partial t}-\frac{uv\tan\varphi}{R}-fv= -\frac{g}{R\cos\varphi}\frac{\partial}{\partial \chi}(\zeta_s-\overline{\zeta})-\frac{F_b}{\rho D}+A_h\nabla^2 u \quad (2)$$

$$\frac{\partial v}{\partial t}+\frac{u}{R\cos}\frac{\partial v}{\partial \varphi}+\frac{v}{R}\frac{\partial v}{\partial \varphi}+\frac{u^2\tan\varphi}{R}+fu=-\frac{g}{R}\frac{\partial}{\partial \varphi}(\zeta_s-\overline{\zeta})-\frac{G_b}{\rho D}+A_h\nabla^2 v \quad (3)$$

where:

t is time;

χ, φ are longitude and latitude;

ζ_s is the elevation of the sea surface above its undisturbed level;

$\overline{\zeta}$ is the equilibrium tide;

u, v are the components of the depth-mean current, **q**;

F_b, G_b are the east-west and north-south (respectively) components of bottom stress, τ_b.. τ_b is defined as $k\,\rho\,\mathbf{q}|\mathbf{q}|$ where k is the friction coefficient;

D is the total water depth (= h + ζ, where h is the undisturbed depth);

ρ is the density of sea water (a constant);

R is the radius of the Earth;

g is the acceleration due to gravity;

f is the coriolis parameter ($f = 2\omega\sin\varphi$, where ω is the rotation rate of the Earth);

A_h is the horizontal eddy viscosity coefficient.

The initial conditions used for the model were no disturbance of the sea surface and no currents:

$$\zeta(\chi,\varphi)_{t=0}=u(\chi,\varphi)_{t=0}=v(\chi,\varphi)_{t=0}=0$$

The model is driven by the conditions along the open sea boundary (indicated in Figure 1.1). The model is capable of using two ways of handling the open boundary, the radiation condition and the elevation-specified condition. With the radiation condition ζ_s, u, and v are specified along the boundary, whereas

with the elevation-specified condition, as the name implies, only ζ_s is specified, with u and v being calculated (using equations 2 and 3 above). It is obviously advantageous to use the radiation condition if possible, since the model is being driven with three independent variables, instead of the single variable being used in the elevation-specified condition.

Effect of the presence of an ice shelf

Tides have been studied in the vicinity of George VI Ice Shelf (Potter and Paren, 1985) and on Ross Ice Shelf (Williams and Robinson, 1980). In previous models of tides beneath Antarctic ice shelves (MacAyeal, 1984b, 1979; Genco et al., 1994; Le Provost et al., 1994; see Chapter 1) water column thickness has been used instead of bathymetry beneath the ice shelves. In addition, MacAyeal (1984b, 1979) doubled the friction coefficient beneath the ice shelf, in order to take account of friction at the base of the ice shelf.
Use of water column thickness rather than bathymetry will tend to increase the importance (*magnitude*) of frictional effects. This will happen because a reduced depth of water through which the tide propagates will require a corresponding increase in velocity in order for the same volume of water to be transported. As a quadratic friction law is used in the model to calculate the bottom stress τ_b, a doubling of velocity will result in a fourfold increase in the magnitude of friction (see p. 8).

Lutjeharms et al (1985) noted that the presence of sea-ice cover lagged the high and low tides by ~0.5 to 1.5 hours, recorded by a BPR in 252 m of water in Atke Bay (71° 3' S 11° 45' W). Godin (1986, 1980) found that at sites around the coast of Hudson Bay, Canada, the amplitudes and phases varied from summer to winter, and concluded that this was due to the presence of sea-ice in winter, the tidal wave being lagged and damped by the effect of increased friction. Further, the data suggests that the presence of sea-ice has the greatest effect in shallow water. Pond and Pickard (1983, p.105) quote that frictional effects should be taken into account up to where the magnitude of the effect is 10% of the Coriolis force, and give a vertical distance of 100

m. as an order of magnitude value. This agrees with Godin's findings from Hudson Bay, where the depth is ~200 m, if one assumes that the frictional effects are of the same magnitude at each interface (sea floor and ice-ocean interface). On the other hand, a calculation of the thickness of the Ekman layer in the real ocean (from Pond and Pickard, 1983, p109) gives a value of ~18 m. The range of "normal" values for vertical eddy viscosity (not included in the model) of 10^{-1} to 10^{-5} gives a layer thickness of 2 - 100 m. The model implicitly assumes that the two boundary layers do not interact and that the effect upon the whole water column may be represented by simply summing the friction of each interface. The situation where the water column thickness is less than the thickness of the boundary layers cannot be taken into account because the model is depth-integrated, nor is it apparent from the literature what the effect of interacting boundary layers would be.

Potter and Paren (1985) found that tidal records from George VI Ice Shelf contained higher order (i.e quad & quin diurnal) tidal components and deduced that these constituents were produced by the response of the ice shelf to tidal forcing. Holdsworth (1977, 1969) investigated the bending of ice shelves by tidal motion, near to the grounding line (within a few ice shelf thicknesses of where the ice shelf ceases to float and the ice is supported by the sea floor) and found that the ice shelf could be modelled as a viscoelastic beam. Doake (1978) estimated that globally significant amounts of tidal energy might be dissipated by this mechanism, along the grounding line of all Antarctic ice shelves. However, Vaughan (1994) has found that ice shelf bending can also be modelled as an elastic beam, which would indicate that no energy is being dissipated within the ice shelf. Nevertheless, the effect of ice shelf bending upon the water column may be to cause dissipation of tidal energy, and the model takes no account of any effects resulting from ice shelf bending.

To summarise, the literature shows that there are two ways in which the presence of an ice shelf may affect the tides:

(a) presence of another frictional surface.

(b) flexure of the ice shelf near to the grounding line.

(a) can be easily included in the model, by increasing the friction coefficient after the manner of MacAyeal (1979, see also Le Blond (1991)). This is a simplification which may not work well if there are significant areas of shallow (less than 100 m) water, where the frictional boundary layers interact. (b) represents a more difficult problem, since in the zone where the ice shelf is bending the surface of the ocean (the ice-ocean interface) is not behaving hydrostatically. Vaughan (1994) has described the relation between vertical displacement and distance from the grounding line for a bending ice shelf:

$$\omega = A_0(t)[1 - e^{-\beta x}(\cos \beta x + \sin \beta x)]$$

where

ω is the vertical displacement of the ice shelf;

$A_0(t)$ is the tidal displacement beyond the hinge zone;

x is the distance from the grounding line;

β is the spatial wave number, given by

$$\beta^4 = 3\rho_{sea} g \frac{1 - \nu^2}{Eh^3}$$

υ is Poisson's Ratio;

E is Young's modulus;

h is the thickness of the ice shelf.

No attempt has been made to include the effects of ice shelf bending in the model, though it would be an useful extension of the model to include it.

The structure of the model

Because of the way in which this model has developed, it has a rigid structure which compartmentalises different parts of the modelling process into different programs. Figure 2.1 is a diagram of the structure of the way in which a model run is carried out. The model is essentially in three parts:

a) SET UP: a pre-processing program which defines the model domain in a memory-efficient form. It is at this stage that open boundaries, or any other properties of the model domain (such as presence of ice shelf) are defined.

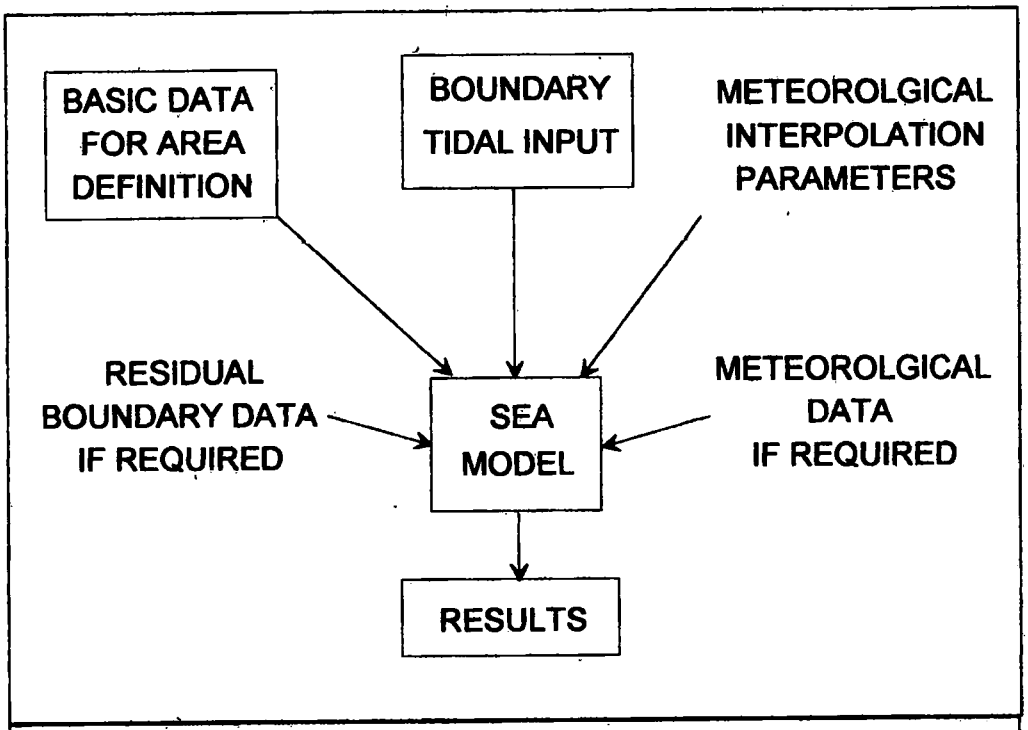

Figure 2.1: *Block diagram of model structure, showing component programs and data sets. Unboxed text indicates parts of Flather model not used for Weddell Sea tidal model.*

b) MODEL: the actual model, which uses the depth-averaged form of the Navier-Stokes equations, with the non-linear advective terms treated by the method of angled-derivatives. This is covered fully in Flather (1994).

c) HARMONIC ANALYSIS: analyses the model output by a least squares method, for the amplitude and phase of specified constituents. The number of constituents for which a given record can be analyzed is given by the Rayleigh criterion, which states that any two neighbouring constituents should be separated by at least one complete period over the length of the record:

$$T = 1/(f_1 - f_2)$$

where $T \equiv$ length of the record;

$f_1, f_2 \equiv$ frequencies of the two neighbouring constituents.

For example, S2 has a period of 2.0000 cycles/day, while M2 has a period of 1.9322 cycles/day. The Rayleigh criterion indicates that:

$$T=1/(2.0000 - 1.9322) = 14.75 \text{ days}$$

is the length of record required to separate S2 and M2.

Modifications made to the Flather model.

Various changes were made to the normal modelling process to take into account the presence of the ice shelf. At the very first stage of using the model this was done by simply using water column thickness for the model domain instead of bathymetry, as done by MacAyeal (1979). This produced encouraging results, but did not reflect the presence of an extra frictional surface at the ice-ocean interface. I therefore modified the SET UP program so that the model domain included a "depth of ice-water interface" derived from the ice shelf thickness by the (hydrostatic) formula (Vaughan, 1994):

$$D_{ice\text{-}water} = 0.892 H_{ice} - 17$$

where $D_{ice\text{-}water} \equiv$ depth of ice-water interface in metres; $H_{ice} \equiv$ ice shelf thickness in metres; 17 is an empirical "firn correction" to account for the lower density of the snow and firn which compose the top 30-40 metres of the ice shelf.

Within the SET UP program, water column thickness was calculated from the bathymetry and ice-water interface depth. A separate value for the basal friction over the area of the ice shelf (defined as area where $D_{ice\text{-}water} > 0$ m) could be specified.

THE MODEL DOMAIN

The domain which is being modelled is shown in Figures 2.2 (a) and (b), which give the bathymetry and ice shelf thickness for the area. The relation of this area to the rest of the Antarctic was shown in Figure 1.1. The model covers an area from 60° S to 85° S and 10° W to 90° W, with open boundaries at 60° S, 60° W and 10° W. The domain is a regular grid in latitude and longitude and has 120 nodes in longitude and 150 in latitude giving a grid-size of 40' longitude (37.0 km at 60° S and 6.5 km at 85° S) and 10' latitude (18.5 km). Both data sets are derived from the Map of subglacial and seabed topography (1994) with the bathymetry to the north of this being taken from

the DBDB5 data set (Van Wyckhouse, 1973). There are several points which should be noted about both sets of data.

Bathymetry data. The bathymetry data is poorly known in the southern and western parts of the Weddell Sea, with (for instance) the continental shelf break being placed too far west in the DBDB5 data set (LaBrecque and Ghidella, 1992). Also there is very little information on the bathymetry in the very southern part of the ice shelf covered region, with contour lines in this region being little more than educated guesswork (Smith, 1995). Thus the true depth of the sea bed trough running along the very southern edge of the Filchner-Ronne Ice Shelf is not known, nor its true extent confirmed, though work currently being undertaken by the British Antarctic Survey has partially answered this question. Smith (1995) has also shown that the ETOPO-5 data set (National Geophysical Data Center, 1988) which is derived from DBDB5 contains false "bulges". A similar feature was apparent in the DBDB5 data, being a topographic rise located at 74° S 60° W which had a minimum depth below sea level of 10 m. Such a feature, would be expected to have shown its presence by iceberg groundings and/or a disruption in the sea-ice cover. As neither effect has been reported for this area, I have concluded that this feature is an artefact of the data set, and have manually removed the extremely shallow data point, leaving a topographic rise with an arbitrary minimum depth of 100 m., this being (approximately) the shallowest depth that would not cause iceshelf groundings on this topographic feature.

Ice shelf thickness. The thickness of the ice shelf has been mainly derived from "raw" (non-retracked) ERS-1 altimeter heights (Sievers et al, 1994), which extends to 82°S and as such does not cover all of the ice shelf covered area. In addition the radar altimeter is unable to track the surface when passing over steep surface slopes or broken terrain (such as caused by crevassing). Both of these conditions tend to occur where the ice shelf runs aground at the coast or on ice rumples. The original intention was to fill in any gaps in the ice shelf thickness data with data from an earlier, Russian data set (Pozdeyez and Kurinin, 1987) which was produced from ice surface

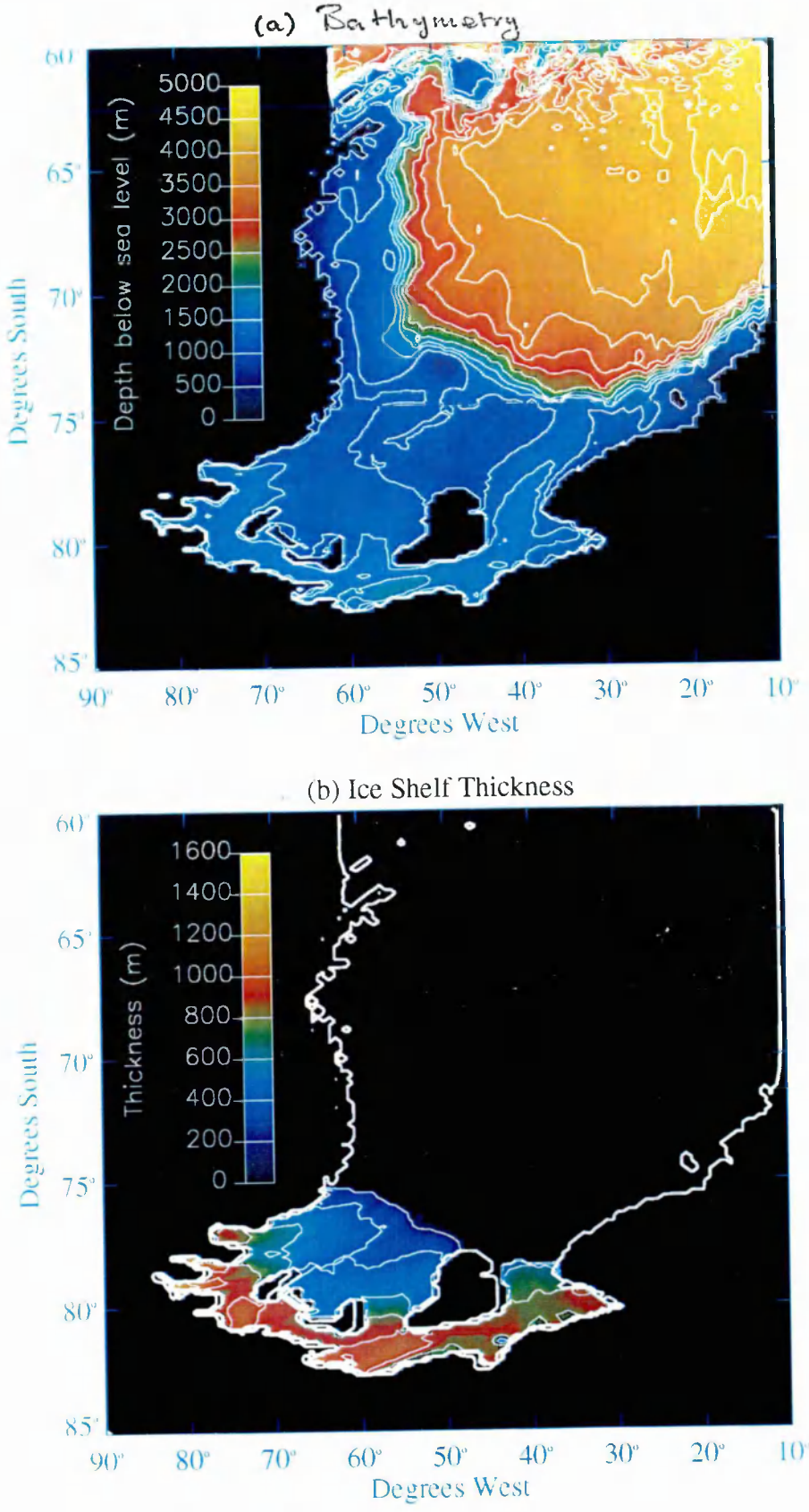

Figure 2.2: Model domain datasets:

(a) Bathymetry ;

(b) Ice Shelf Thickness.

heights measured using a satellite positioning system (Magnavox). However this proved to be impossible since in some places the Russian data disagreed with the bathymetry data set, indicating an ice thickness which placed the base of the ice shelf below the sea floor. The disagreements occurred in places characterised as ice rumples (Topographic Map (Satellite Image Map), 1993), where the shelf is flowing over a piece of topography and is temporarily grounded. Because ice rumples often have relatively steep surface slopes compared with the rest of the ice shelf, and are often crevassed, ERS-1 data is more likely to be unreliable. However for similar reasons, and because ice rumples are more common the further south one goes (towards the grounding line the ice gets thicker and hence is more likely to run aground) these are also the places where the Russian data coverage is thinnest, and sometimes non-existent (Pozdeyev and Kurinin, 1987, Figure 1). Instead, the gaps in the "raw" ERS-1 data were filled by interpolation between the last ERS-1 data points, and known values of ice thickness at the coastlines (Map of subglacial and seabed topography, 1994), subject to a minimum of 50m due to the quoted errors in the map.

The time step used within the model was 60 seconds. The size of the time step can affect the stability of the model and is chosen according to the following criterion:

$$\Delta t < \frac{\Delta s}{\sqrt{2gh}}$$

where Δt is the time step;

Δs is the distance between the grid nodes;

g is acceleration due to gravity;

h is water column thickness.

This is known as the Courant-Friedrichs-Lewy criterion.

The minimum distance between grid nodes is 6.5 km in the southern part of the model domain. Using this value for Δs in equation 5 indicates that a 60 second time step will provide stability if $h > 5$ m. In fact the minimum depth

permitted within the model (for example at coastlines) was 50 m in the ice-shelf covered portion (which includes all of the southern part of the model domain) and 10 m in the rest of the model domain, these being the respective uncertainties in bathymetry.

OPEN BOUNDARY DATA

The only data available to drive the model along the chosen open boundary (see Figure 1.1) are global ocean tide models. Two of the most commonly used global ocean tide models (Andersen, 1994) are those of Schwiderski (1980) (hereafter SCH), and Cartwright & Ray (1990) (hereafter CR). The data from such global models is commonly used to drive regional tidal models (Flather, 1993) such as the one presented here. SCH is a finite-difference model with tidal records assimilated into the model. Unfortunately, most of the tidal records were from sites in the N.E. Atlantic, and none were from the Atlantic sector of the Southern Ocean, or the Weddell Sea. SCH may therefore be expected to have relatively high errors in the Weddell Sea. CR is an analysis of sea surface heights from the TOPEX/Poseidon mission covering the globe from 75°N to 75°S. Satellite altimeters are unable to obtain accurate surface heights when sea-ice is present because of the radically different surface characteristics of sea-ice. As the Weddell Sea always has extensive sea-ice coverage (Sea-Ice Climatic Atlas, 1985) CR amplitudes and phases will have higher errors in the Weddell Sea.

Figure 2.3 is a comparison between SCH and CR, in both amplitude and phase, along the open boundary of the model, for each of the four main constituents. It can be seen that the two models agree quite well over most of the open boundary, though there are significant differences in amplitude of the diurnal constituents, of the order of ~ 20 cm (50%) for any given constituent

Figure 2.3 (a): Amplitudes of SCH and CR constituents along open boundary

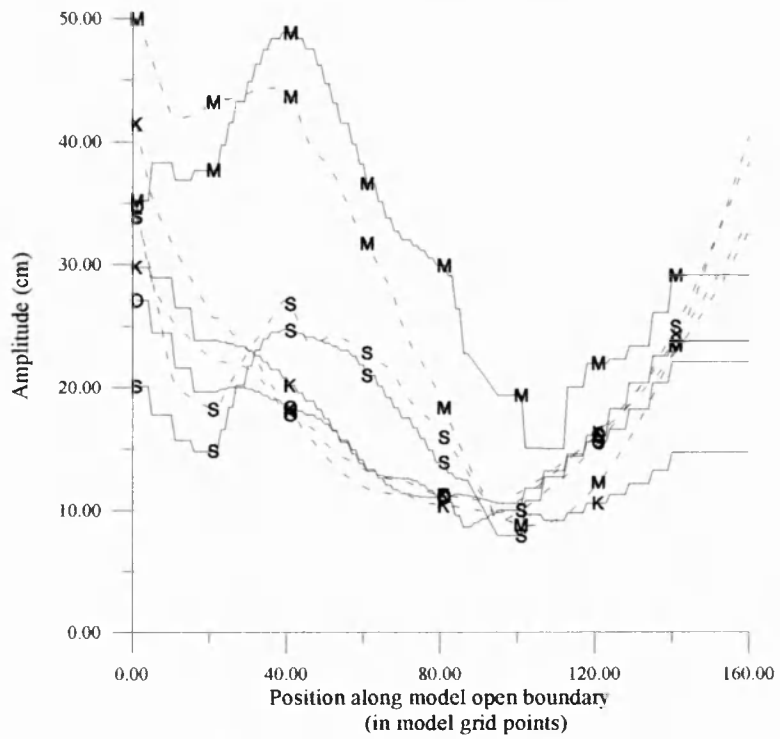

Figure 2.3 (b): Phase of SCH and CR constituents along open boundary

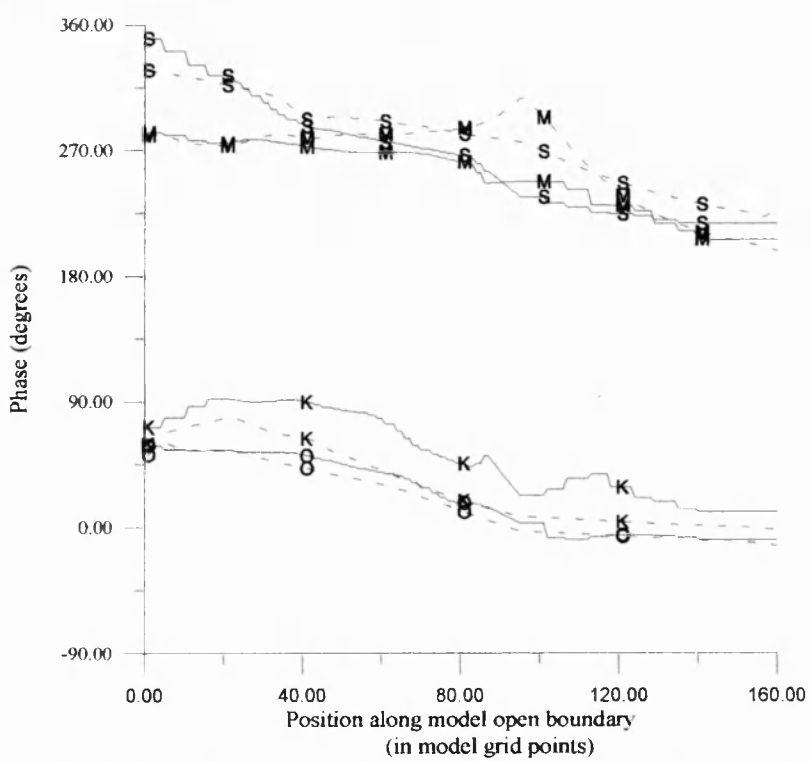

Figure 2.3: Amplitude and phase of open boundary data. Dashed and solid lines represent SCH and CR derived data. Letters in bold indicate tidal constituents: O is O1; K is K1; M is M2; and S is S2. Position along open boundary starts at intersection of open boundary with Antarctic Peninsula.

SUMMARY

In this section, I have given a brief description of the model and the modifications made to it in order that it might be applied to an ice shelf covered area. I have also described the data sets from which the model domain and open boundary conditions were derived. The model domain is poorly known in the south and west of the model.

In the next chapter I will go through the known tidal records from the area, and then describe the ability of an initial model run to fit these records.

Chapter 3:

The standard model run
and its fit to known data for the area.

INTRODUCTION

Chapter 2 described the numerical model, its associated boundary conditions and the model domain. In this chapter I will describe the known tidal data for the southern Weddell Sea, and present the results of a "standard" model run, which uses simplistic assumptions about the effect of the ice shelf upon the tides.

TIDAL RECORDS FOR THE WEDDELL SEA

In order to produce an accurate model of the tides of the Weddell Sea, some knowledge of the actual tides is required against which to check the model results. Figure 3.1 shows the positions (marked with "+") of all available data sets, plotted on a contour map of the bathymetry for the area of the Weddell Sea which is of interest. Table 3.1 gives the amplitude and phase of each of the main four constituents for all sites. The sparsity of data is because of the conditions of heavy pack ice which prevail in the Weddell Sea, making it difficult to deploy oceanographic instruments, and even harder to recover them. Further, the presence of an ice shelf in the southern part of the Weddell

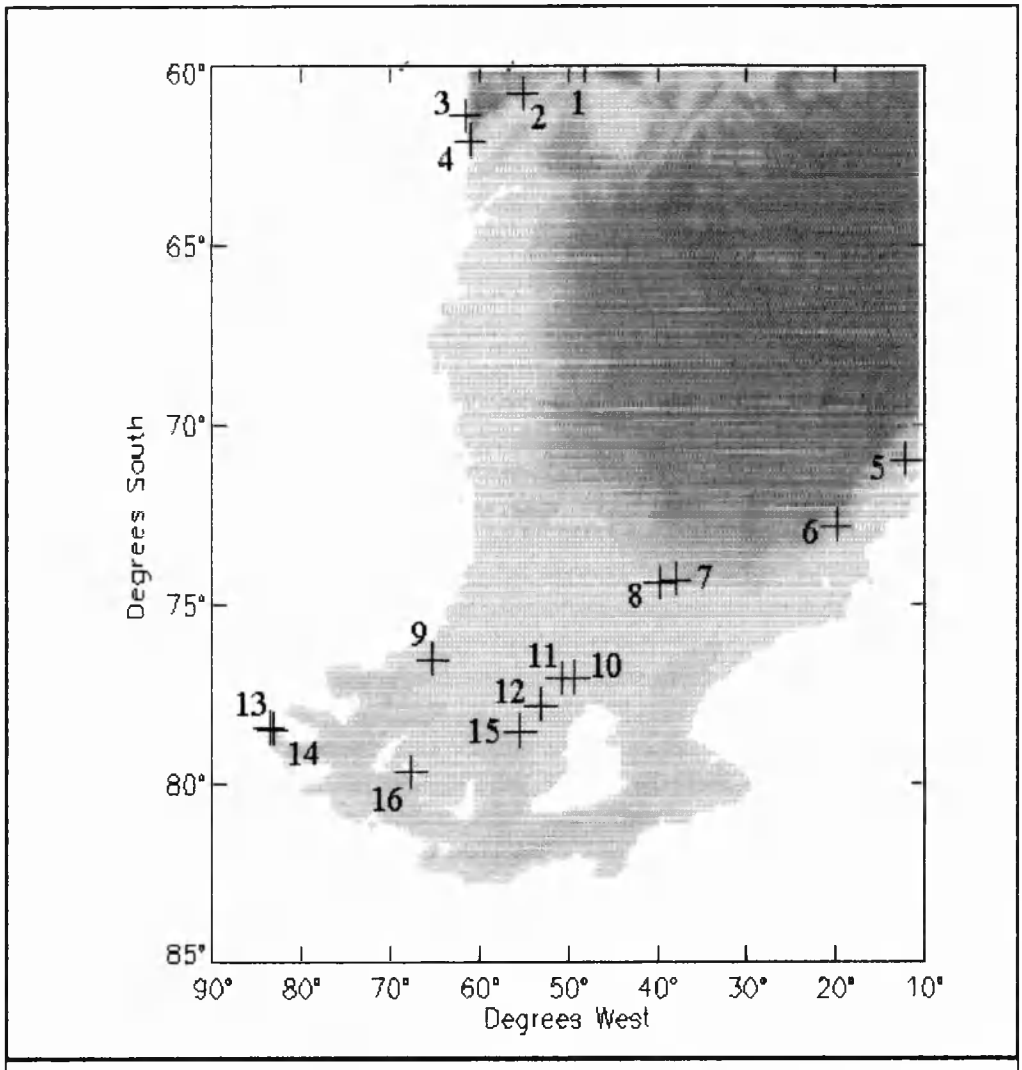

Figure 3.1: *Locations of sites in Weddell Sea to be used for comparison with model output. Numbers refer to text and to Tables 3.1, 3.2, and 4.1.*

Sea, has prevented measurements of tidal motions by the "normal" means of Bottom Pressure Recorders or current meters, though such measurements are planned in the near future.

The data from sites 1 to 8 and 10 were collected using bottom pressure recorders, and none are in shallow water. Sites 9 and 11 to 16 were all measured using either gravimeters or tiltmeters, and are comparatively short records. Taking each site in turn:

1) to 3) were long deployments using multiple sensors with identical (within experimental uncertainty) results from different sensors. The length of the records and the agreement between different sensors at a given site suggest that the data sets are very reliable.

4) was a year long deployment as part of the ISOS Drake Passage Experiment, analyzed at POL.

5) and 6) were collected by Alfred Wegener Institut (AWI). Both are long records, with low variances, and are consistent with another site just beyond the model boundary.

The proximity of sites 1 to 6 to the model boundaries will allow comparison with the boundary condition data, to provide an estimate of any errors in the SCH or CR models. The present model's accuracy should be highest at these sites, if the boundary conditions are accurate.

7) and 8) were collected by University of Bergen. Site 7 is a very clean 30 day record and site 8 is a noisier year long record. These sites can be used to ensure that the best-fit model for the ice shelf area is also a good fit over the rest of the Weddell Sea, and does not produce any unphysical effects in the centre of the model domain.

10) a 4.5 day record from a BPR deployed, by the University of Bergen, 10 km from the ice front. This is the most southerly direct measurement of the height of the water surface, which has been analyzed for 8 constituents using the response method (Munk and Cartwright, 1966). This method assumes that the different tidal constituents are related to each other in the same way as the equivalent equilibrium tidal constituents, which allows analysis of shorter records than is possible using a least squares approach. However, Cartwright (1979) has shown that the relationship between equilibrium constituents can change in the vicinity of an ice shelf, so the response method may not have been an appropriate analysis method. Standard errors for the analyzed constituents may be up to 6% in amplitude and 3° in phase.

9) is a 14 day gravimeter record (Doake, 1992), from a location on Ronne Ice Shelf. It is expected to be the ice shelf site which the model is most likely to be able to reproduce well, given that it is well away from the coast and associated grounding line effects. However, gravimeter measurements are prone to instrumental problems, and are an indirect measure of tidal motion.

Table 3.1: Amplitude and Phase of the four largest tidal constituents in the Weddell Sea

Site	Lat (S)	Long (W)	O1		K1		M2		S2		Record Type[1]	Reference
			H(cm)	G(°)	H(cm)	G(°)	H(cm)	G(°)	H(cm)	G(°)		
1	60° 3'	47° 5'	19	50	15	67	42	268	21	299	P	Smithson (1992)
2	60° 51'	54° 43'	20	48	19	67	44	276	22	322	"	Smithson (1994)
3	61° 28'	61° 17'	22	51	23	72	33	268	15	342	"	"
4	62° 8'	60° 41'	24	54	25	73	32	280	17	351	"	"
5	71° 3'	11° 45'	29	352	27	358	47	193	33	223	"	Smithson (1992)
6	72° 53'	19° 37'	31	359	29	5	57	220	39	242	"	"
7	74° 23'	37° 39'	31	6	37	17	58	242	39	262	"	"
8	74° 26'	39° 24'	33	7	32	6	53	233	39	264	"	"
9	76° 42'	64° 53'	51	36	41	147	93	92	54	161	G	Doake (1992)
10	77° 7'	49° 3'	29	23	29	23	49	280	29	295	P	Smithson (1992)
11	77° 8'	50° 30'	22	132	20	264	27	224	16	291	G	Doake (1992)
12	77° 53'	52° 45'	17	93	16	231	23	144	8	245	G	"
13	78° 30'	83° 20'	45	63	50	55	165	72	104	98	G	"
14	78° 33'	82° 58'	35	63	38	55	126	72	79	98	T	"
15	78° 37	55° 8'	14	127	15	219	35	159	25	182	G	"
16	79° 44'	67° 21'	34	58	32	72	137	61	81	89	T	"

[1] P - Bottom Pressure Recorder; G - Gravimeter; T - Tiltmeter.

11), 12) and 15) were short (5-9 day) gravimeter records collected by the University of Munster. Despite their proximity to each other the analyzed constituents for these sites are inconsistent. This may be due to instrumental error, or to the shortness of the records. Therefore at least one of these records is unreliable (see Appendix B, page 77).

13), 14) and 16) are sites (Doake, 1992; Smith, 1992; Stephenson, 1986) near the grounding line of the ice shelf, at Rutford Ice Stream (Sites 13 and 14) and Doake Ice Rumples (Site 16). Sites 13) and 16) are 43 day tiltmeter records, near to the point where the maximum change in surface slope occurs. Site 14 is a 4 day gravimeter record which was analyzed assuming that the phases and relative amplitudes were the same as for site 13 (Doake, 1992), though Site 14 is approximately 20 km downstream of Site 13. The amplitudes at Site 14 are ~30% higher than at Site 13. This may reflect a problem with the conversion of tiltmeter angles to vertical distances, i.e. an incorrect bending profile being used, implying that the assumption that the bending of the ice shelf can be modelled as an elastic beam (Vaughan, 1995; Smith, 1991; Stephenson, 1986) may not be true very close to grounding lines.

Because there are so few sites, it will be difficult to know when a good fit has been achieved by the model. This problem is particularly severe in the area of the Filchner and Ronne Ice Shelves, where the data is not only sparse but can be contradictory (for example Sites 11, 12 and 15), and the tides may be expected to show more complicated and rapid variability than in the northern parts of the Weddell Sea. This is caused by the increased effect of friction in shallower water columns, in addition to any effects on the tides that result from the presence of the ice shelves. Also, all data on the ice shelves were collected using gravimeter and tiltmeter measurements, both indirect methods of obtaining vertical tidal motion. Gravimeter measurements require the application of several corrections in order to produce a measure of surface motion, and will also measure the Earth and ocean load tide. Tiltmeter measurements require assumptions about the way in which an ice shelf bends near a grounding line. The measured angle of tilt is converted into a sea

surface height by simply extrapolating from the grounding line (where by definition there is no tidal signal) through the tiltmeter site (Smith, 1991) to a point at which the ice shelf is freely bending. By definition this requires that the measurements are made within the region where the motion of the sea surface is affected by ice shelf bending. Thus all of the records from the ice shelf area (sites 9 and 11 to 15) are likely to be more inaccurate than the pelagic sites (1 to 8), in addition to being, in general, much shorter records.

From the above tidal records it is possible to draw some broad conclusions about the "shape" of the tides in the Weddell Sea, as Doake (1992) did for the S2 constituent. Doake (1992) showed that the S2 tidal wave travels around Berkner Island, entering the sub-ice shelf cavity at Filchner Ice Front and exiting from Ronne Ice Front, being retarded by 360° by its passage under the ice shelf. This, in effect, makes the coast of Berkner Island and the coast of the mainland form a channel along which the semi-diurnal tides may travel as a progressive wave. This is unlikely to be the case as such features are more normally confined to long, narrow channels such as estuaries (Pond and Pickard, 1983, p274). Since the narrowest channel under the ice shelf is over 100 km. wide it is more likely that the tides will behave as a Kelvin wave with one or more amphidromic points in the vicinity of the ice shelves. Therefore the most important conclusion that can be made from the data is that there should be an amphidrome(s) in the semi-diurnal constituents, and that this amphidrome(s), is probably located in the central part of the embayment where the Filchner and Ronne ice shelves are. In order to have achieved a reasonable qualitative fit the model must at least replicate this feature for the semi-diurnal tides, though the precise location of the amphidrome(s) is unable to be determined with the presently available data.

Method of analysis of model results.

As stated in Chapter 1, one of the aims of this project was to produce a data set to correct ERS-1 satellite altimeter data. Therefore, the difference between modelled sea surface height and true sea surface height

(reconstructed from the analyzed constituents for the chosen sites) was of great interest. Thus, I synthesised year long time series of sea surface height for each site, from the constituent data for each site, and from the analyzed constituent data from the model output, and deducted the former from the latter to obtain the error in modelled sea surface height. The standard deviation or r.m.s. error, σ_n, of the difference between the two models is then calculated:

$$\sigma_n = \sqrt{\frac{\sum_{i=0}^{n} (y_i - y_i')^2}{n}}$$

where $y_i \equiv$ reconstructed analyzed sea surface heights;

$y_i' \equiv$ reconstructed modelled sea surface heights;

$n \equiv$ length of the record (in this case 8760 hours);

i indicates a particular hour of the year.

This data is then displayed as a graph of σ_n for each site and variation in model parameters (if any). The accuracy required for the altimeter correction is of the order of 0.5 m (D.Mantripp, pers comm). 0.5 m may represent a significant proportion of the tidal range, for example near to an amphidrome. The quality of fit of the model will be also measured by the normalised error:

$$\sigma_n{}^* = \frac{\sigma_n}{\sum_{j=1}^{4} A_j}$$

where $A_j \equiv$ the amplitude of constituent j, taken from the tidal data (see Table 3.1).

THE STARTING POINT: DOUBLED FRICTION UNDER THE ICE SHELF.

As mentioned in Chapter 2, the base of the ice shelf is assumed to represent another frictional surface to the tides. The simplest assumption about friction beneath the ice shelf is that made by MacAyeal (1979, 1984b), which is that the base of the ice shelf has the same value of friction as the sea floor, and so

in this depth-averaged model, the bottom friction is doubled. It is with this assumption that the investigation of the tides of the Weddell Sea began, using doubled friction under the ice shelf, and with open boundary conditions derived from SCH.

The model run was for 22 model days, with output being stored from day 8 onwards. This provided a 15 day time series at each point within the model, which was sufficient for the analysis of the four constituents O1, K1, M2, and S2 with which the model was being driven. The analyzed results of the model run are shown in Figures 3.2 to 3.5. Figure 3.2 -3.5 show co-amplitude and co-phase plots of the four main constituents. Figure 3.6 (a) shows a graph of the r.m.s. error, between model and data, plotted against the latitude of each of the sites described above. Figure 3.6 (b) shows the r.m.s. error as a percentage of tidal range (calculated as the sum of the amplitudes of the four constituents being modelled). Table 3.2 contains the modelled amplitudes and phases at each site, and the differences between these values and the true amplitudes and phases (see Table 3.1 for site data).

The model results:

Figures 3.2 to 3.5 show that the modelled tides have reproduced the expected features of the structure of the tides. In particular, Figures 3.4 and 3.5 show that there are two semi-diurnal amphidromic points in the southern Weddell Sea.

Figure 3.6 (a) indicates that the model is not a very good fit to the data at most of the sites. Better fits are achieved at sites closer to the open boundary (1-6) and further away from the influence of the ice shelf. The level of error at these sites reflects that the SCH data set is not a very good match to the true tides along the open boundary, and that it becomes worse towards the south. Quoted residual errors for the tidal records at these sites (Smithson, 1992) are in the range ~0.01- 0.1 m. This represents the minimum error that the model may be able to reproduce. It is only at Sites 1-4, all of which lie on or near to the open boundary that this level of error is achieved.

In Figure 3.6 (a) a large step increase in error occurs at the continental shelf edge (Sites 7 and 8) because of the increase in amplitude. Sites 7 and 8 are

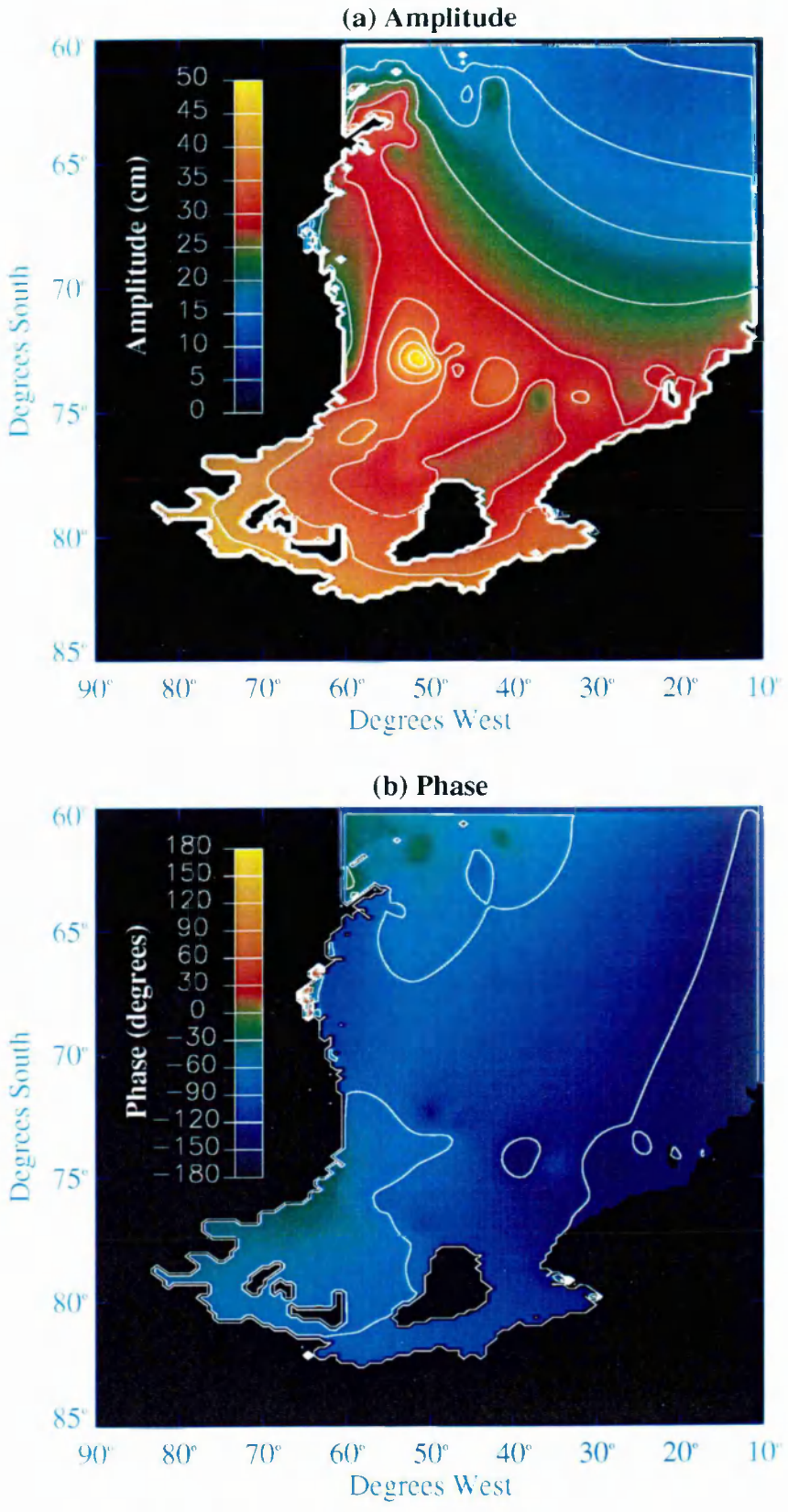

Figure 3.2. The modelled O1 constituent:

(a) Amplitude in centimetres;

(b) Phase in degrees.

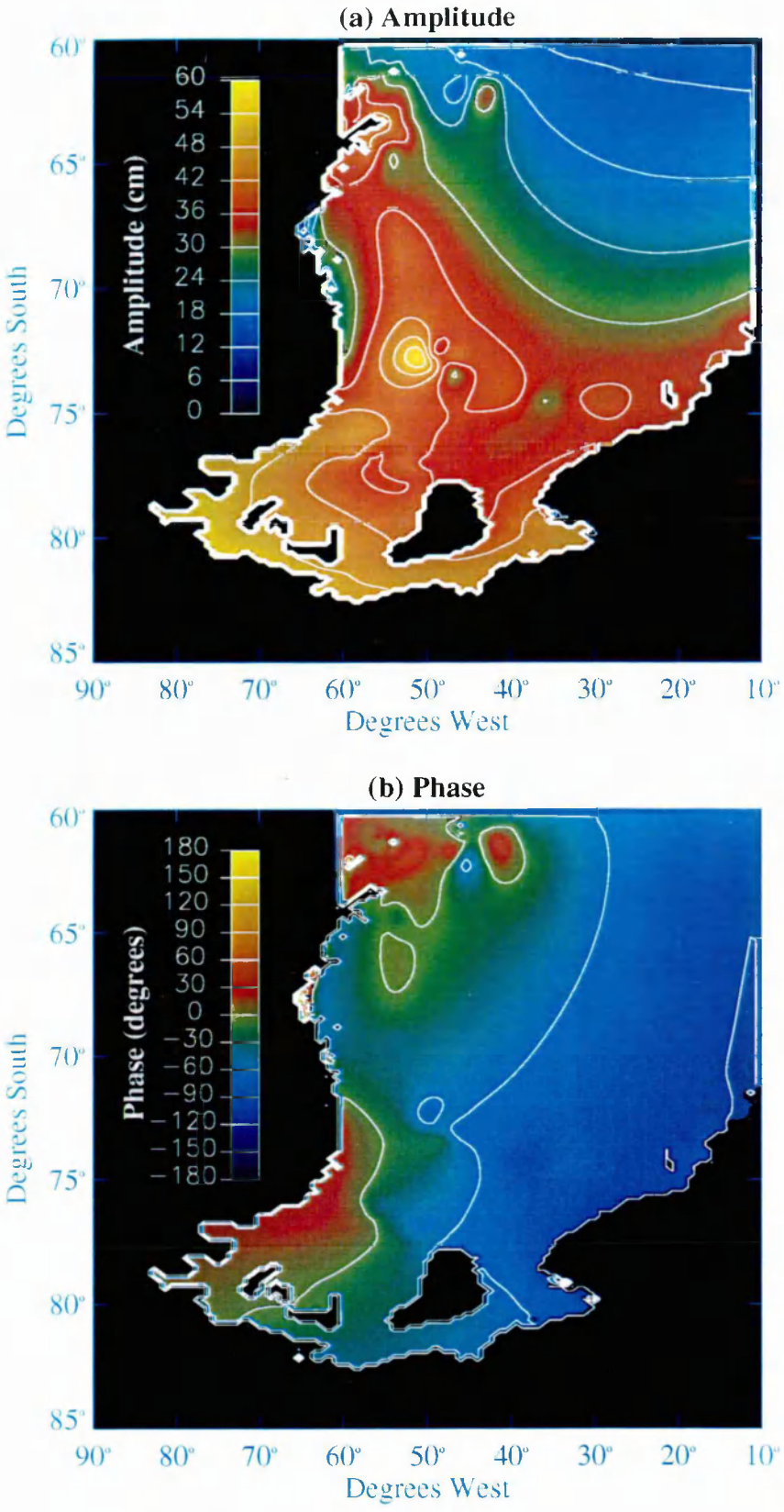

Figure 3.3. The modelled K1 constituent:

(a) Amplitude in centimetres;

(b) Phase in degrees.

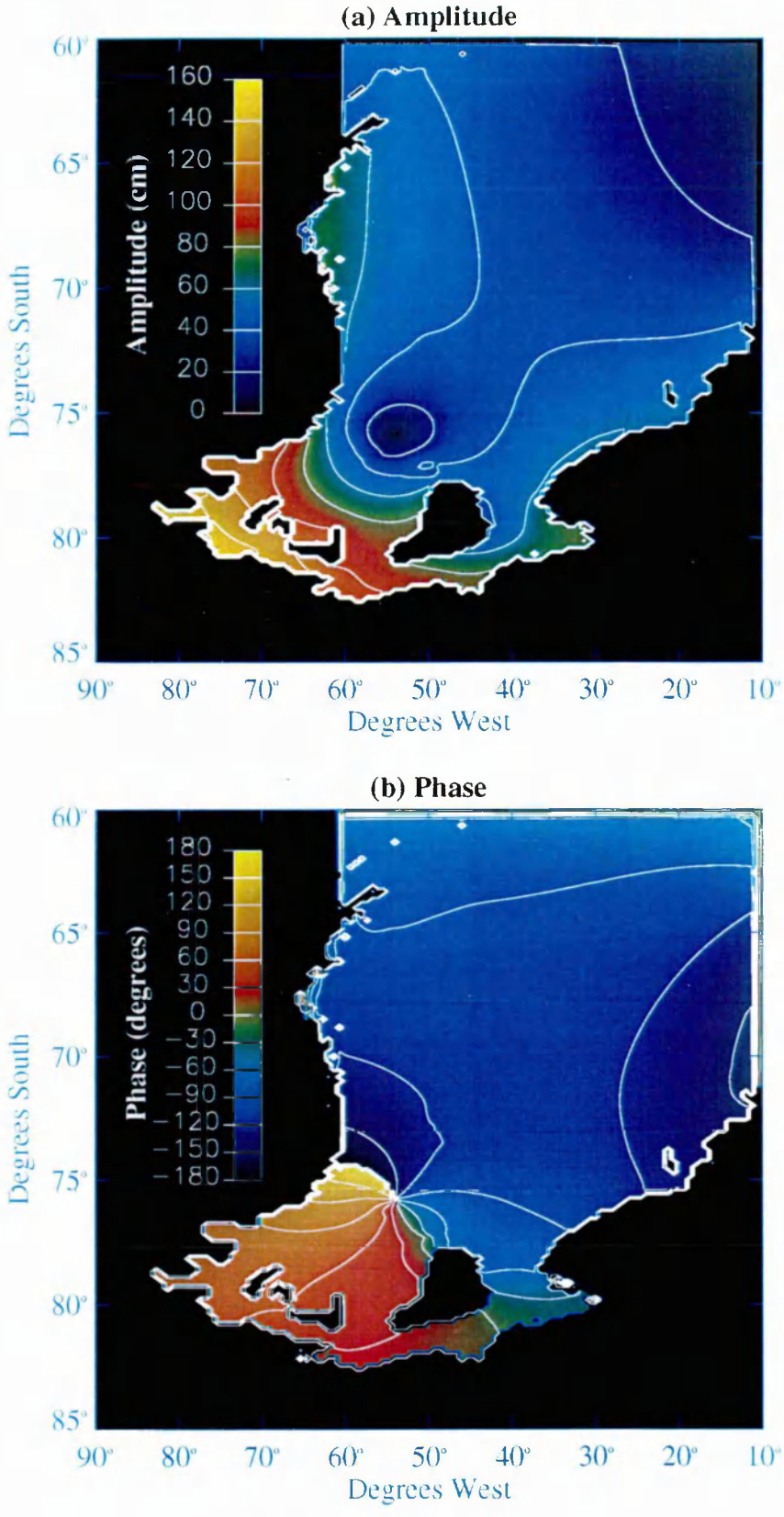

Figure 3.4. The modelled M2 constituent:

(a) Amplitude in centimetres;

(b) Phase in degrees.

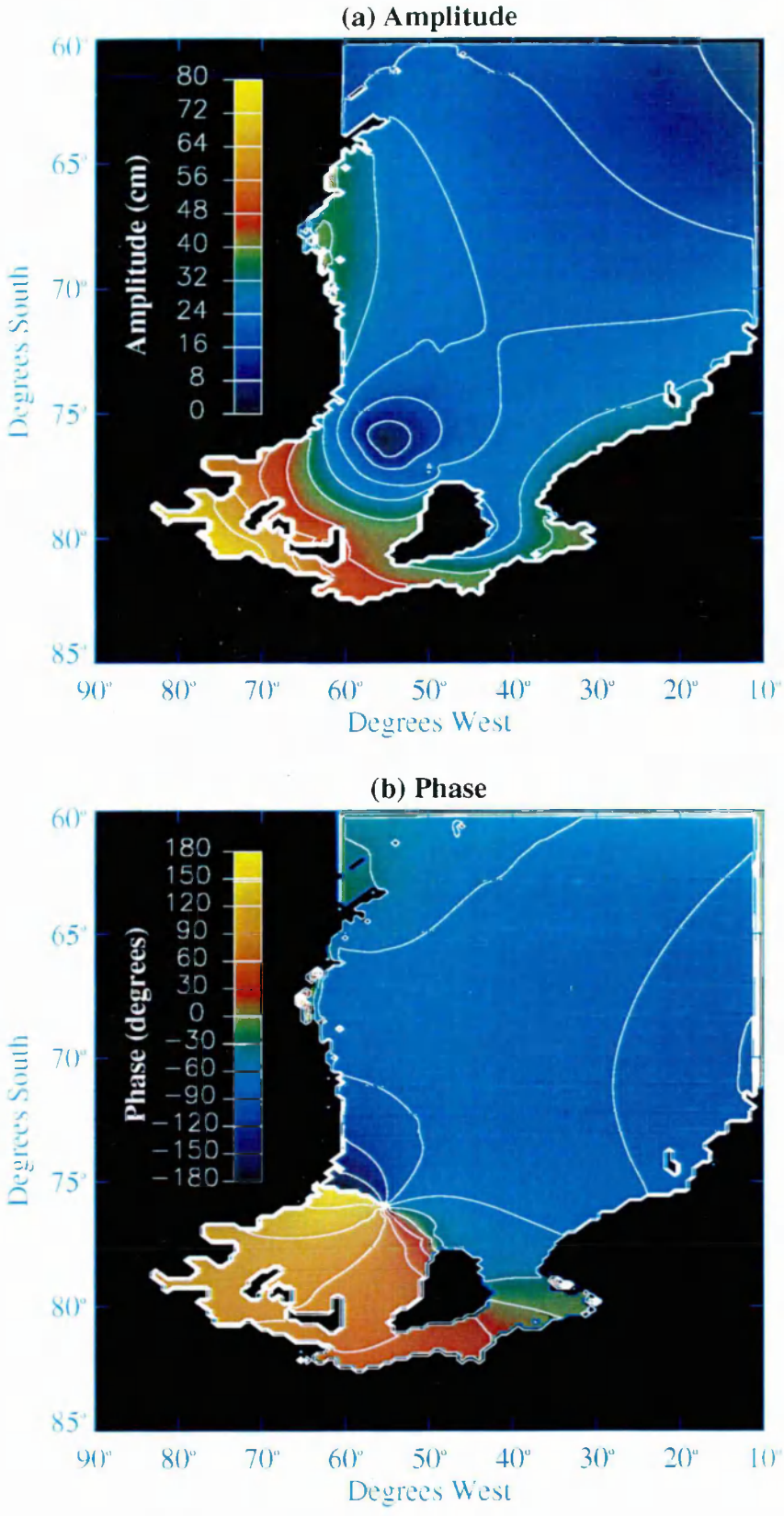

Figure 3.5. The modelled S2 constituent:

(a) Amplitude in centimetres;

(b) Phase in degrees.

only ~20 km apart but there is a three fold difference in error between them. Wavelike features are visible in the maps of the diurnal constituents (Figures 3.2 and 3.3) appearing as a sequence of peaks and troughs in amplitude and as closed phase contour lines. These features seem to reflect variations in the bathymetry along the continental shelf break, and so are probably topographic (continental shelf) waves (Kowalik, 1994). Because the bathymetry is poorly known, it is likely that the difference in error between the two sites is caused by inaccurate model bathymetry.

For the remaining sites (9-16), it is apparent that there is a general trend of increasing error with latitude (S). Sites 11,12, and 15 all have much higher errors than any of the other sites (see Appendix B). Figure 3.6 (b) shows that for these sites the r.m.s. error is greater than the tidal range of the main four constituents, indicating that the model is in partial anti-phase with the recorded phases. Given the inconsistencies in measured phases (see Table 3.1) between these sites, and the better agreement between the model and other nearby sites such as Site 10, the cause of the high levels of error is almost certainly due to a problem with these records, and not the model. The lower error at Site 10 may be attributed partly to its proximity to the semi-diurnal amphidrome, and partly to the reliability of the measurement technique used. Equally, the increase in error with latitude for the ice shelf sites can be attributed to the increase in amplitude of the semi-diurnal constituents. This is shown by the small gradient of the dashed line in Figure 3.6 (b) which is the best fit percentile error for all sites, excluding Sites 11, 12 and 15. The decrease in quality of fit with increasing latitude is in keeping with the variation in accuracy of the SCH data set (see Table 3.3). Site 13 has a lower error and higher quality of fit than Site 14. A comparison of the modelled amplitudes indicates that they agree very well with the gravimeter data. Given this agreement and the problems with amplitude from tiltmeter data, only Site 13 will be used for investigations of the model's sensitivities.

Figure 3.6 (a): Variation in r.m.s. error with latitude

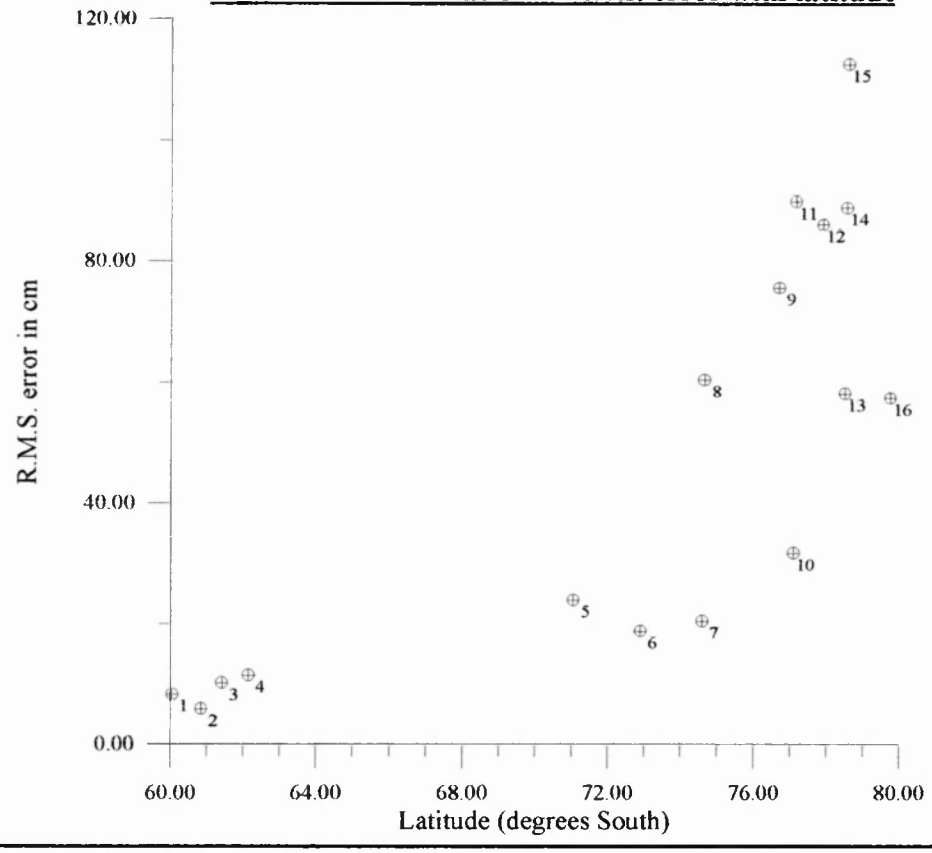

Figure 3.6 (b): Variation in % error with latitiude

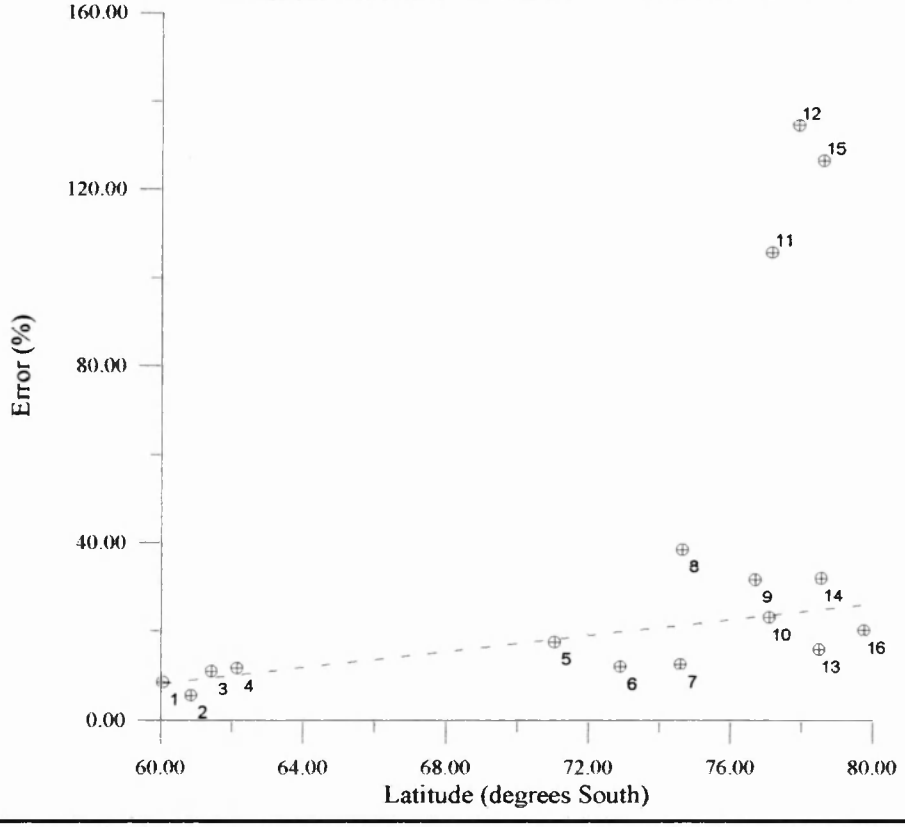

Figure 3.6: *Variation in r.m.s. and percentage error with latitude for "standard" model run. Numbers refer to Sites in Table 3.1.*

The structure of the semi-diurnal tides:

Comparing Figure 3.5 (b) with the map of S2 drawn by Doake (1992) (Figure 3.7) it can be seen that the model essentially reproduces the main features, with an amphidrome centred on the ice front of Ronne Ice Shelf, approximately halfway between Berkner Island and the coast of the Antarctic Peninsula. The positioning of this amphidrome may explain the poor quality of fit at Site 10. It can be seen by comparing Table 3.2 with Table 3.1 that the main contribution to the difference in sea-surface heights at this site is due to the phases of the semi-diurnal constituents. The site is close enough to the amphidrome that small changes in the position of the amphidrome can have a large effect on the phase, but have a small effect on amplitude, because lines of equal phase are very close together near an amphidrome (by definition). In addition the model shows that there is a rapid change in phase of the semi-diurnal tides near to the ice front. This is caused by the rapid change in depth at the ice front, and was found by Doake (1992) in his production of a co-tidal map of S2 phases (Figure 3.7). The main difference between Figures 3.5 (b) and 3.7 is in the location of the semi-diurnal amphidrome. This results from Doake (1992) including Sites 11, 12, and 15 (see Appendix B) in his analysis of the S2 tide. The S2 phase data for these sites are the most self-consistent in the variation of phase between the different sites (see Table 3.1).

The structure of the diurnal tides:

The diurnal constituents have a fairly simple structure, closely resembling a standing wave, except in the region of the continental shelf break, where a pattern of successive peaks and troughs in amplitude, coincident with closed co-phase lines, can be seen. This is characteristic of topographic waves (Kowalik, 1994). Examination of the topography in the area (Figure 2.2 (a)) reveals large variations, such as where Filchner Depression reaches the continental shelf edge. As mentioned in Chapter 2, the DBDB 5 data set has large variations in bathymetry along the shelf break, including depth values which were clearly erroneous and had to be manually edited. The known variations in bathymetry on the shelf edge (e.g. Middleton et al, 1982) indicate

Table 3.2: Amplitude and Phase of the four largest tidal constituents using SCH open boundary data.

Site	Lat (S)	Long (W)	O1		K1		M2		S2	
			H(cm)	G(°)	H (cm)	G(°)	H (cm)	G(°)	H (cm)	G(°)
1	60° 3'	47° 5'	18	44	19	64	44	280	27	296
2	60° 51'	54° 43'	24	52	24	76	43	280	23	314
3	61° 28'	61° 17'	24	55	30	74	42	274	19	321
4	62° 8'	60° 41'	26	56	32	71	42	276	21	323
5	71° 3'	11° 45'	34	350	35	0	45	208	39	266
6	72° 53'	19° 37'	35	355	35	10	53	231	36	261
7	74° 23'	37° 39'	33	356	35	17	49	257	36	278
8	74° 26'	39° 24'	39	355	38	21	47	259	35	280
9	76° 42'	64° 53'	46	54	47	82	98	98	58	123
10	77° 7'	49° 3'	34	16	35	40	52	318	35	334
11	77° 8'	50° 30'	39	16	39	41	48	358	28	14
12	77° 53'	52° 45'	38	33	37	59	55	33	31	55
13	78° 30'	83° 20'	55	45	55	75	182	74	113	98
14	78° 33'	82° 58'	55	45	55	75	182	74	113	98
15	78° 37'	55° 8'	40	35	39	61	79	44	46	67
16	79° 44'	67° 21'	50	40	50	68	154	62	94	85

that topographic waves would be seen in the true tides, if there were sufficient data in this area to resolve them.

The ice shelf sites 9, 10, 13, 14, and 16: It is expected that the errors at these sites are quite large, as explained in the site descriptions above. The quality of fit was expected to be much worse at Sites 13/14 and 16 than at Sites 9 and 10, because ice shelf bending was expected to affect the tides at Sites 13/14 and 16. Figure 3.6 (b) shows that this is not true, with the error at Sites 13, 14 and 16 being 16%, 33% and 21% respectively, compared with 33% and 24% for Sites 9 and 10. However, MacAyeal (1979, Appendix A) showed that ice shelf bending would only become important when the water column thickness is much less than the thickness of the ice shelf. On the Rutford Ice Stream (Sites 13 and 14), where the water column thickness is 600-800 m, with ice shelf thicknesses of 1200-1500 m, this is not true. Site 16, on the Doake Ice Rumples, was expected to be more strongly effected by ice shelf bending, because of the shallowness of the water column and thickness of the ice shelf (Smith, 1991, see Figure 2) fulfilled MacAyeals (1979) criteria for ice shelf bending. However MacAyeal (1979) was considering the case of an ice shelf well away from the coast/grounding line.

CONCLUSIONS

It has been shown that the model has achieved a reasonable fit to the known data at first attempt, reproducing the general structure of the four main constituents in the Weddell Sea, using a simple assumption about how the presence of the ice shelf affects the tides. Overall, modelled tidal heights are within 17 ± 9 % of the known tidal ranges. The model achieves a poorer quality of fit with increasing latitude. It is not clear whether this decrease in quality of fit is due to the presence of the ice shelf or an increasing divergence between the SCH data and the true tides. The high quality of fit achieved for Sites 13 and 16 suggests that processes such as ice shelf bending are not important on the length scales used in the model.

The next chapter describes the investigations of the model sensitivities to variations in the model parameters and domains, to determine if it is possible to improve the fit. Four sites (Sites 11, 12, 14, and 15) were not included in the investigations of the model sensitivities because of the high errors between model results and data found at these sites. Sites 11, 12, and 15 has such high errors that they appeared to be in anti-phase with the model results. In addition the phase data was inconsistent between the sites, given their relative locations. Therefore, I concluded that there was probably a problem with the data from these sites and excluded them from further analyses. Site 14 was located close to Site 13, and the phase data from Site 14 was used in the analysis of Site 13 (Doake, 1992), therefore since Site 13 had lower errors between the model and the tidal data, and was believed to have more reliable amplitude data than Site 14, Site 14 was also excluded from further analyses of the model results.

Chapter 4:

Experiments with the model.

INTRODUCTION

Chapter 3 described the known tidal records covering the area of the Weddell sea to be modelled and the results of a model run using a set of initial assumptions about the effect of an ice shelf upon the tides. Those results led to the records from four Sites (11, 12, 14 and 15) being discarded because of suspected inaccurate values of amplitude and phase. In this chapter I will investigate the effect upon the modelled tide of varying different parameters and boundary conditions, with the two-fold aim of discovering the model's sensitivities and achieving a better fit to the remaining tidal records.

INVESTIGATION OF MODEL SENSITIVITY

The work presented in Chapter 3, has shown that the model can reproduce well the tides in the open ocean, away from the ice shelf, but that close to the ice shelf the quality of fit deteriorates. In order to understand the reason for this deterioration it is necessary to investigate how the model output varies with changes to model parameters/boundary conditions. This should enable a better understanding of how the model fails to accurately reproduce tides for the ice shelf covered area, and also enable a better fit to the data to be obtained in this area. Hopefully this will provide some clarification of what processes are important in affecting the propagation of tidal waves through an ice-shelf covered area.

The model parameters which were varied were the friction coefficient and the eddy viscosity. As mentioned in chapter 2, the true value of the friction coefficient at the base of the ice shelf is not known. The value for eddy viscosity coefficient was primarily chosen in the original model to give numerical stability (R.A.Flather, *pers. comm.*), and eddy viscosity is commonly quoted (Pond and Pickard, 1989, p.54) as having a range from 10 to 10^5 m^2s^{-1}. Thus it is reasonable to assume that the "best" value for this variable in the model, might be different in an unusual location such as the Weddell Sea. The boundary conditions which could be varied were the tides along the open boundary, because the tides are poorly known in this area, and the geometry of the sub-ice shelf cavity, for which data is very sparse under the ice shelf.

Taking each of the above parameters in turn:

(1) Varying the friction coefficient.

Because of the presence of an extra frictional surface, the coefficient of friction is the most obvious parameter which will be different from the normal open ocean conditions in the sub-ice shelf regime. Furthermore, it is not clear what value the friction coefficient will have underneath an ice shelf. What work that has been done on ice-ocean interfaces has been restricted to sea-ice (Godin, 1986; Murty & Polavapurov, 1979), which is a very different environment from that beneath an ice shelf, where there are no effects from wind, swell, and the large variations in ice-ocean interface topography caused by the presence of "sails" and rafting within the pack of sea-ice. Thus the friction parameter is one which may be varied with relative freedom. The initial assumption used in Chapter 3, that was also made by MacAyeal (1979, 1984b) and LeBlond (1991), was to double the friction coefficient underneath the ice shelf. However this is not necessarily the correct value, and even if it were and the open boundary conditions were exactly correct, the modelled tides could still vary from the observed tides (ignoring any failures in the way the model reproduces the tides) because of the presence of sea-ice in the Weddell Sea. Work by Godin (1986) and Lutjeharms et al (1985) in the

Arctic, which was discussed in Chapter 2, has shown that the seasonal variation in sea-ice cover in Hudson Bay causes changes in the amplitude and phase of tides beyond the edge of the pack ice. Because the extent of sea-ice is much greater in the Weddell Sea, it might be expected that the effect of the variation in sea-ice would be proportionately greater in the southern Weddell Sea. This suggests two different ways of varying the friction coefficient:

a) varying the friction coefficient applied to the sub-ice shelf.;

b) varying the coefficient applied to the whole model domain.

If the variation in sea-ice cover does have a major effect on the modelled tides, then a) represents the situation during the Austral summer, when the sea-ice cover is restricted to the western part of the Weddell Sea (Sea-Ice Climatic Atlas, 1985), while b) represents the situation in midwinter when heavy pack ice covers the whole of the Weddell Sea.

The friction coefficient, at each interface, that was used in Chapter 3 was 0.0025 (Ramming and Kowalik, 1980, p.17). The variation of the friction coefficient took the form of applying a multiplier to the friction coefficient. Values of this multiplier were 0.1, 1, 2, 4, 10, 25, 50, and 100. Thus a multiplier of 2 represents the model run presented in Chapter 3, and a multiplier of 1 represents zero friction at the ice-ocen interface.

Results from varying the friction coefficient.

a) Over the ice shelf region.

Figure 4.1 summarises the results with a plot of the r.m.s. errors of each site for each run. It is apparent that at sites 1-7, the r.m.s. error between modelled sea surface height and "measured" sea surface height is insensitive to variations in sub-ice shelf friction, which is to be expected if the sites are all sufficiently far from Filchner-Ronne Ice Shelf to be unaffected by it, and close enough to the open boundary to be dominated by that.

The variation in error at Site 8 may be due to the topographic wave train, that is generated by the continental shelf edge, being altered. It is more likely to be due the general decrease in the amplitude of the tide that occurs with increasing friction, so that the quality of fit remains roughly constant.

Figure 4.1: Variation in r.m.s. error with varving sub-ice shelf friction coefficient

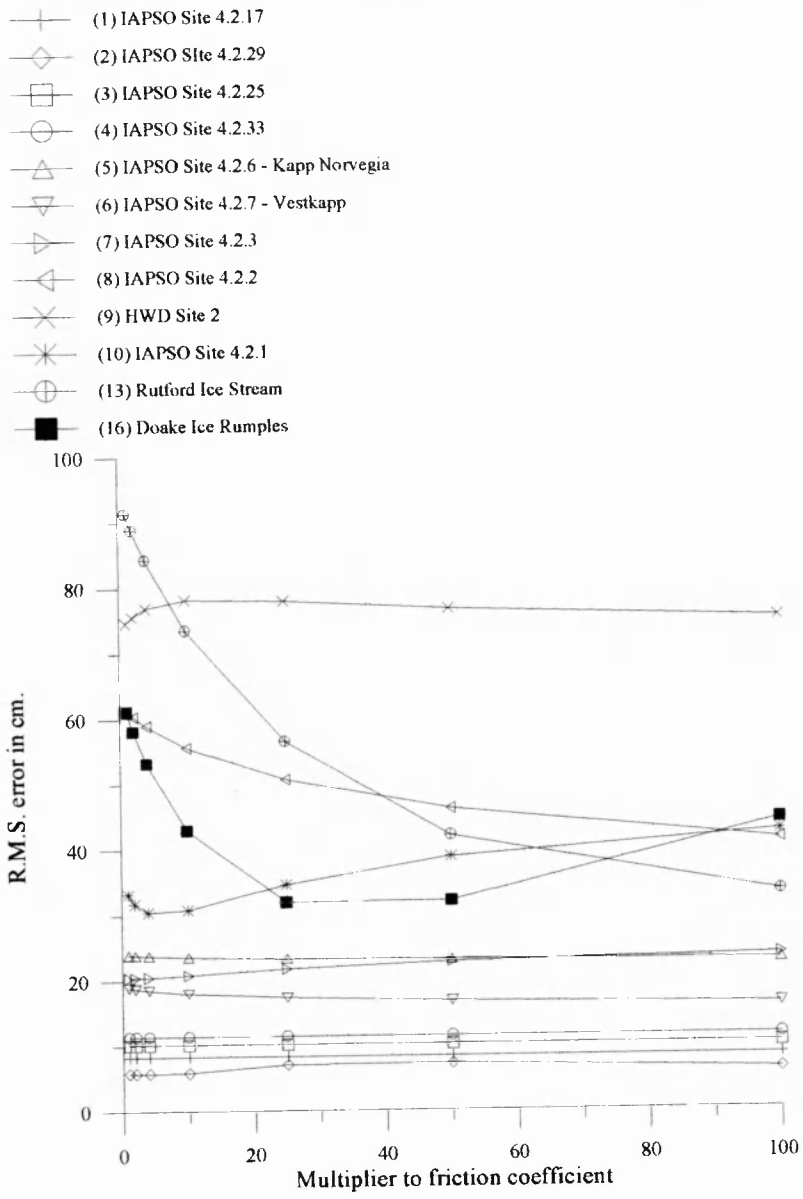

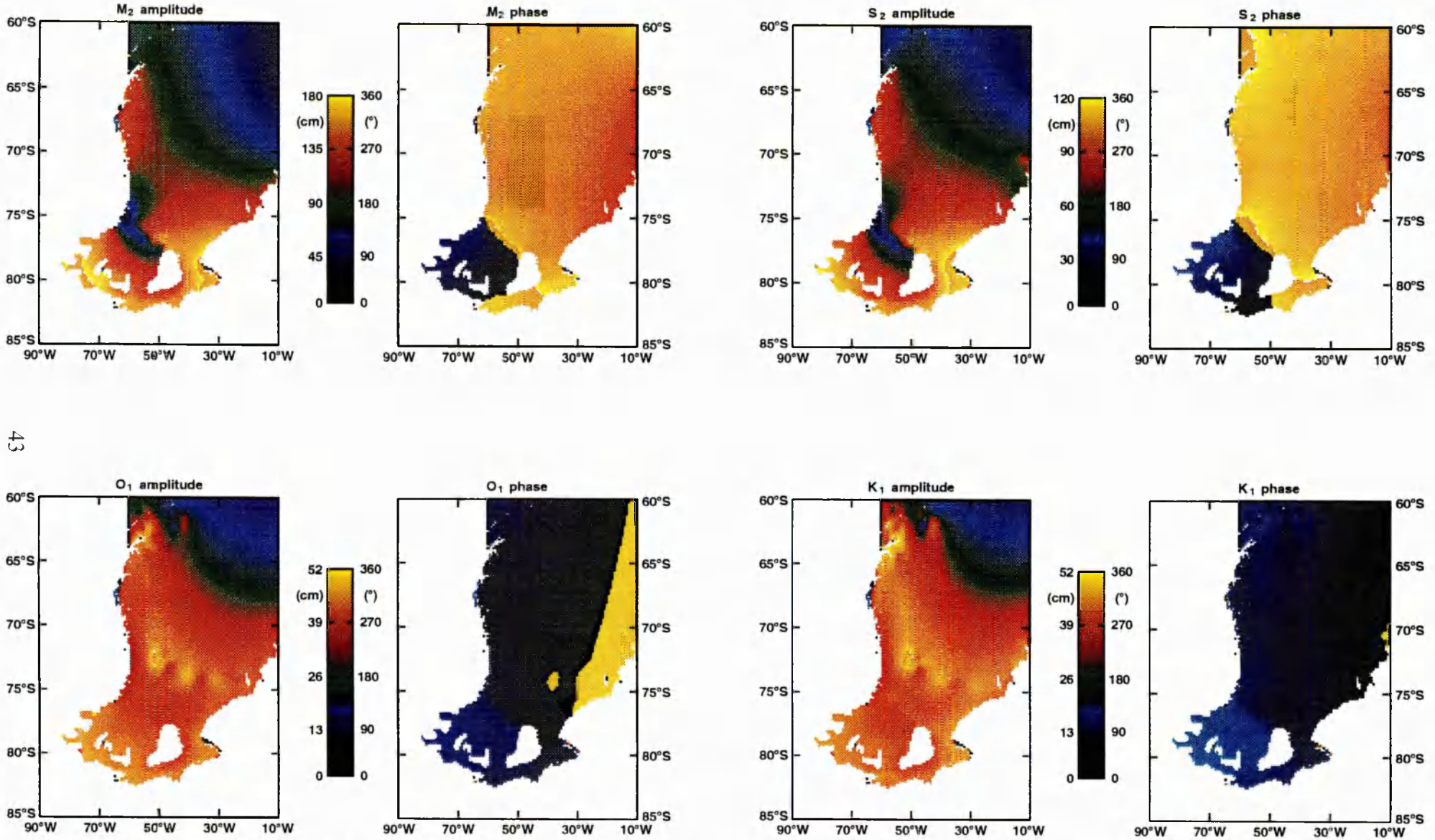

Figure 4.2: *Amplitude and phase plots for all four constituents using a sub-ice shelf friction coefficient of 0.125 (50 times greater than for the standard run in Chapter 3).*

Figure 4.3: Position of M2 amphidrome along Ronne Ice Front

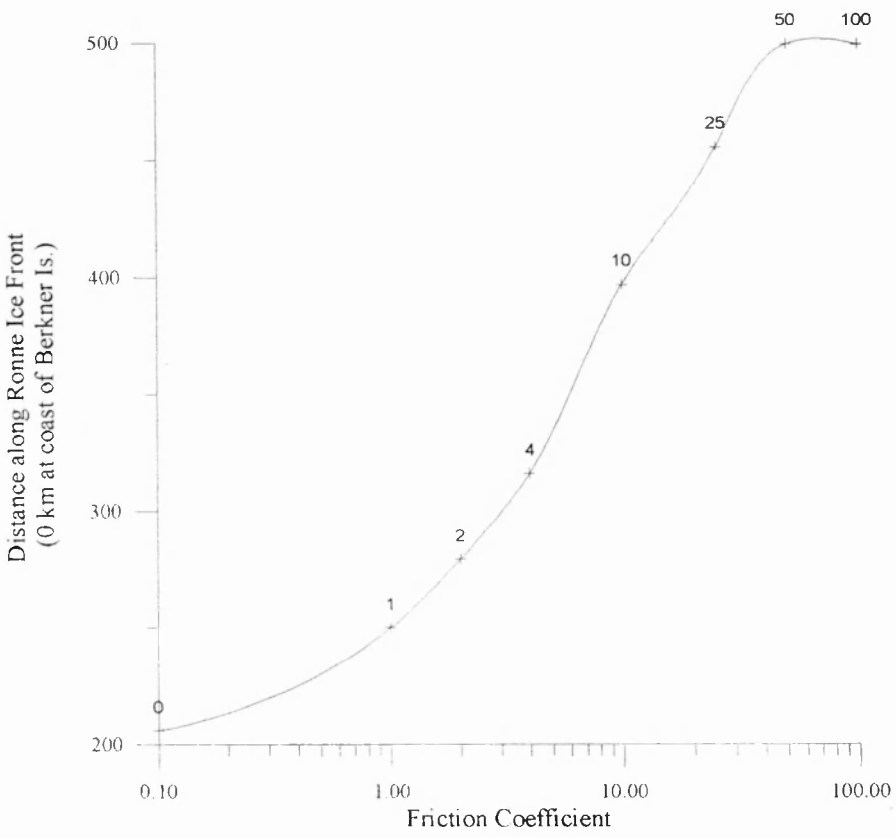

The variation in error at Sites 9 and 10 is probably due to the change in location of the amphidrome with increasing friction. Figure 4.2 shows co-amplitude and co-range plots for all four constituents when the friction coefficient is 0.125 (i.e. multiplier = 50) . It can be seen that the semi-diurnal amphidrome is now adjacent to the coast of the Antarctic Peninsula, but that its position is still coincident with the ice front. The position of the amphidrome always appears to lie on the ice front, and Figure 4.3 shows a graph of the distance from the coast of Berkner Island of the M2 amphidrome against the logarithm of the friction coefficient. Sites 9 and 10 provide contradictory information about the location of the amphidrome. The minimum error between model and data for Site 9 was found using a friction multiplier of 0.1 (Figure 4.1), implying that the amphidrome is located closer to Berkner Island than indicated on Figures 3.4 and 3.5. The minimum error at Site 10 was found using a friction multiplier of 4, implying that the

amphidrome is located closer to the Antarctic Peninsula. As Site 10 is a more reliable data source (see Chapter 3, page 20), and has generally lower errors, the likelihood is that the amphidrome is located somewhere in the middle of the Ronne ice front.

Sites 13 and 16 show very similar behaviour, with the error between the model and the site data decreasing rapidly as friction is increased, reaching minimum values at friction multipliers in the range of 25 to 50. The distribution of tides shown in Figure 4.2 make it unlikely that the minimum is a result of the amphidrome being in a more correct position, as the amplitude and phase contour lines have roughly the same geometry, no matter what value of friction coefficient is used. Further, the difference between modelled and measured amplitude and phase for each constituent are different for the two sites. This implies that there is something about these sites that the model cannot reproduce, and that this is a problem with the model physics rather than an inaccuracy in the open boundary conditions. Because both of these sites are near to grounding lines, the obvious conclusion is that the increase in friction is representing (or partly compensating for) the effect that the bending of the ice shelf has upon the tides.

b) Over the whole model domain.

It can be seen from Figure 4.4 that varying the friction over the whole domain produces a similar pattern of variation in errors as changing the friction coefficient over the ice shelf. Figure 4.4 confirms the indication from Chapter 2, that the effects of the presence of sea-ice in the Weddell Sea do not need to be considered in order to reproduce the tides accurately. Furthermore, the r.m.s. error is generally higher in Figure 4.4 than Figure 4.1 for the sites on the ice shelves. The r.m.s. error for the other sites is approximately the same as above, but decreases slightly with increasing friction. This indicates that applying an increased friction over the whole Weddell Sea does nothing to improve the model's fit, and therefore can be ignored.

Figure 4.4: Variation in r.m.s. error with varying friction over whole Weddell Sea

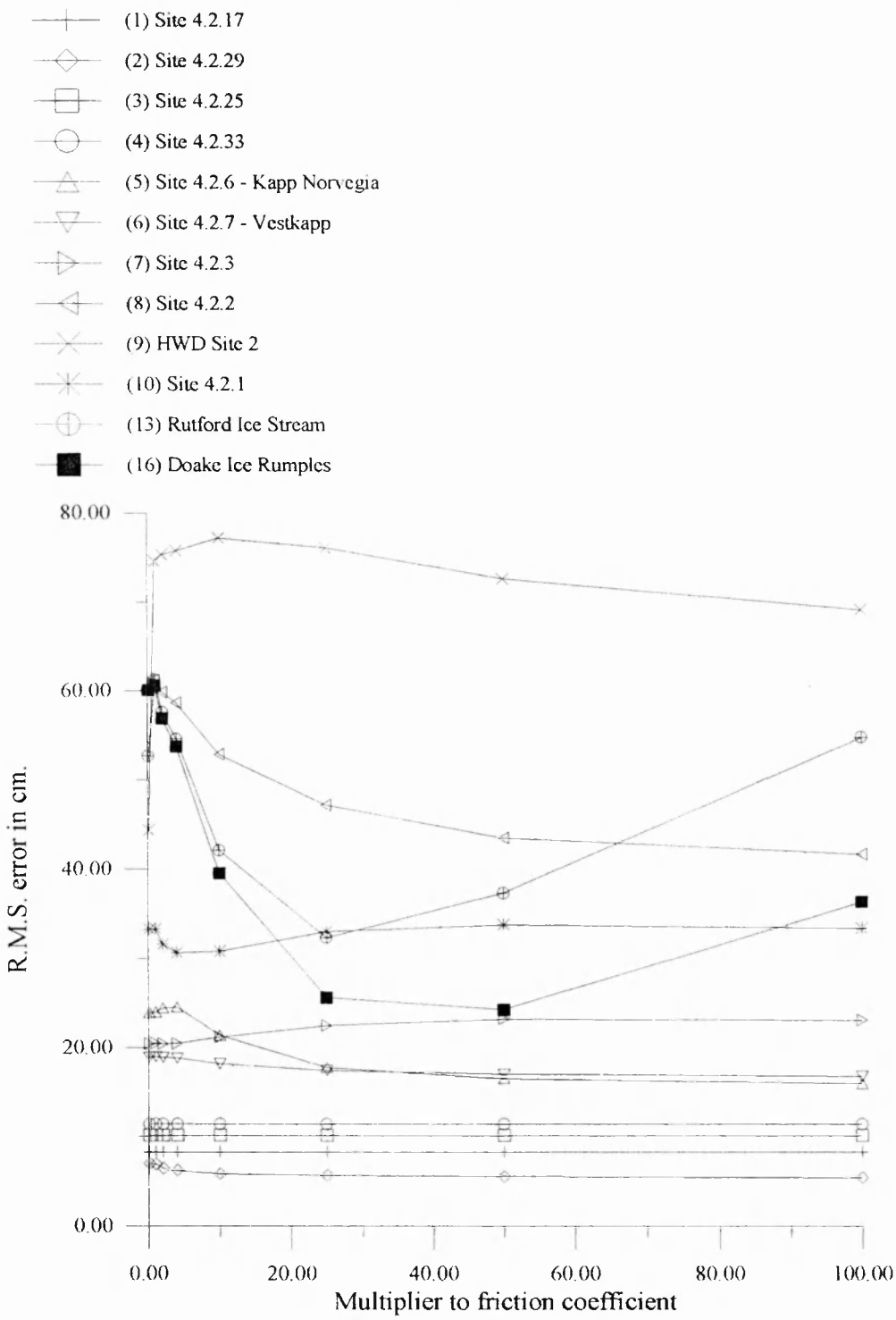

Comparing the situation in the Weddell Sea with that for Hudson Bay as described by Godin (1986) where the presence of sea-ice lags and damps the tide, the main difference is the greater depth of the Weddell Sea compared to Hudson Bay (~4000 m versus ~200 m, (The Times Atlas Of The World, 1994, Plate 97) see also Figure 2.2 (a)). This greater depth of water might be a reason for the negligible effect of sea-ice upon the modelled tides, because of the relation between depth and horizontal gradients of depth-averaged velocities.

From the equation of continuity (equation **(1)**, page 7) it can be seen that greater water column thickness will lead to smaller horizontal velocity gradients. Similar sized tidal waves propagating through the Weddell Sea and Hudson Bay would result in smaller velocities in the Weddell Sea, because of greater water column thickness in the Weddell Sea. Smaller velocities result in less tidal energy dissipation by friction, and a consequently smaller impact from the presence of sea-ice, because of the cubic relation between velocity and frictional dissipation of energy.

Averaged over time T, frictional dissipation of energy is given by:

$$\frac{1}{T}\int_0^t (\rho k|\mathbf{q}|^3)dt$$

where ρ is the density of sea water;

k is the friction coefficient;

$\mathbf{q}$ is the depth-averaged velocity.

This explanation in consistent with Godin's (1986) comment that the effect of the presence of sea-ice increases with distance from the "open ocean" and with similar observations that Lutjeharms et al. (1985) made in Atke Bay (71° 3' S 11° 45' W) of the high tide being lagged by the presence of sea-ice.

Conclusions from changing the friction coefficient.

The greatest effects from changing the friction coefficient are seen at Sites 13 and 16 which are close to the grounding line of Filchner and Ronne Ice Shelves. Both sites show an improved quality of fit at higher values of friction coefficient, though with the best fit at each site being achieved with different values of friction coefficient. The broad effect of increasing friction is to increase the lagging and damping of the tide, as can be seen from the change in position of the semi-diurnal amphidrome. The improved fit at higher friction coefficients for Sites 13 and 16 indicates that the true tide is particularly lagged and damped in these locations, relative to the standard model run, and that applying a higher friction coefficient over the whole ice shelf can reproduce this. Possible explanations for this particularly localised discrepancy between the modelled and true tide are that the model water column thickness is incorrect, or that there is an effect which is not included in the model. Because the model does not attempt to include the effects of ice shelf flexure, and because of the lack of data about the bathymetry and ice shelf thickness in the southern Weddell Sea (Chapter 2), it is likely that both explanations are equally correct.

(2) Varying the eddy viscosity:

The eddy viscosity in the Flather model is depth-dependent, being a constant (the eddy viscosity coefficient) multiplied by the water column thickness, and represents the dissipation/conversion of energy by turbulence within the water column. The true eddy viscosity in any given water column is unlikely to be constant with depth (Nøst, 1993) as implicitly assumed by the Flather model though it is probably an adequate approximation in deep water where the effects of wind and bottom stress can be ignored. In the model, it has the function of increasing the model's numerical stability in the deep ocean, where the effect of friction is minimal. Because quoted values of eddy viscosity coefficient vary by several orders of magnitude, ideally the modelled eddy viscosity coefficient would also have been varied by several orders of magnitude. However, decreasing the eddy viscosity coefficient below 5 m^2s^{-1}

Figure 4.5: Variation in r.m.s. error with varying eddy viscosity

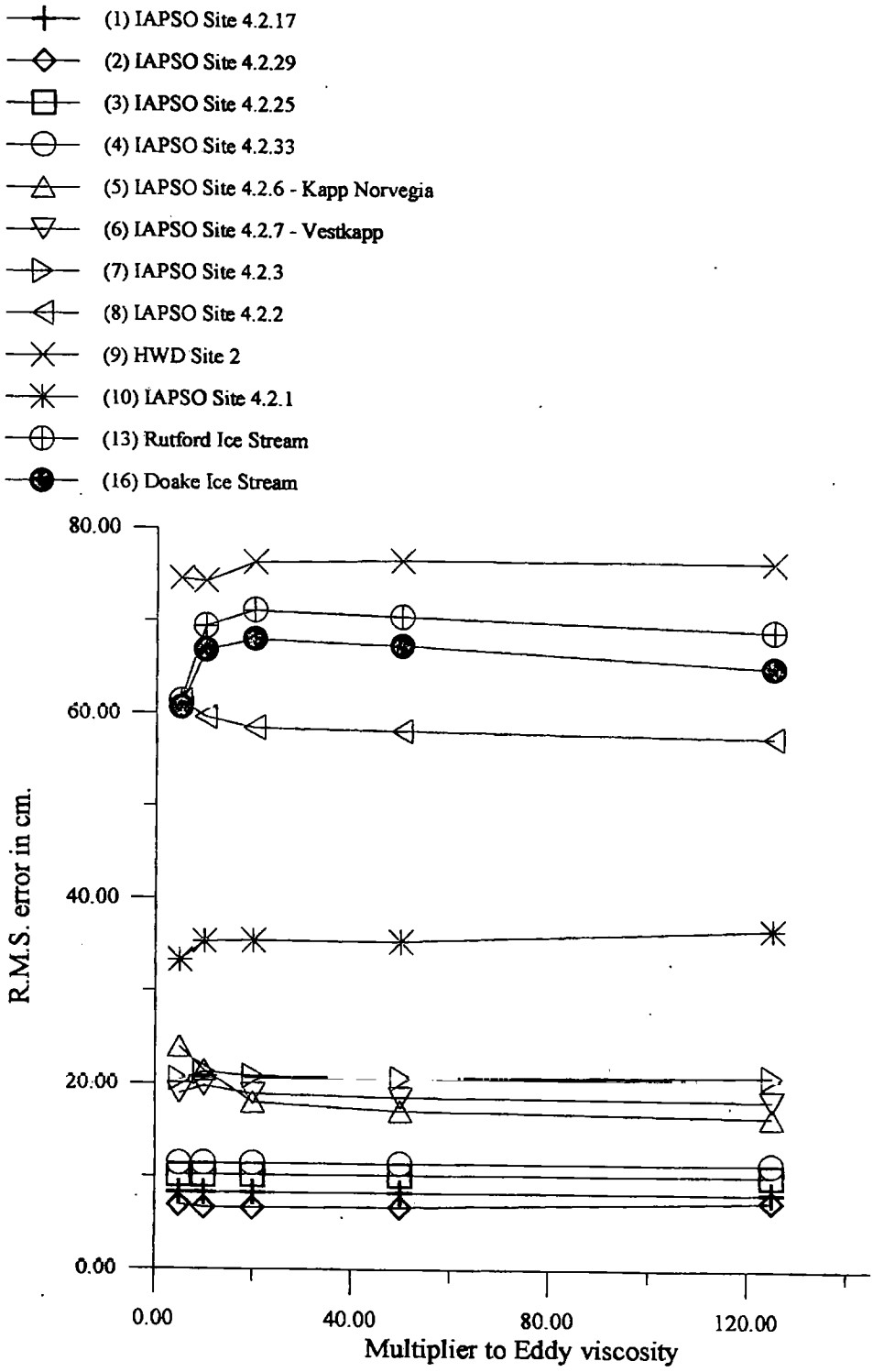

and increasing it above 125 m^2s^{-1} made the model unstable. Therefore, the model was run with only a small range of values.

Results from varying the eddy viscosity

The results are summarised in Figure 4.5. Varying the eddy viscosity did not have a large effect upon the quality of fit at any site. The largest changes were seen at Sites 13 and 16, where the error initially increased with increasing eddy viscosity, reaching a maximum error at an eddy viscosity of 20 m^2s^{-1}, then slowly decreasing with further increases in eddy viscosity. Similar variation was seen at Sites 6, 7, 9 and 10, but Sites 5 and 8 varied in the opposite sense (i.e. initial decrease followed by a slow increase).

Conclusion from varying the eddy viscosity.

The results indicate that the normal value of eddy viscosity is probably the best value, and also confirm that the value of eddy viscosity is important for numerical stability within the model. There is insufficient data to indicate whether a more stable model would show a better fit using a lower (< 5 m^2s^{-1}) value for eddy viscosity.

(3) The geometry of the sub-ice shelf cavity:

As stated in Chapter 2, the bathymetry is poorly known in the southern part of the Filchner-Ronne Ice Shelf, but two of the sites (13 and 16) for which we have reliable tidal data are in this region. For both sites, the modelled semi-diurnal phases tend to lag behind the measured phases (Tables 3.1 and 3.2). The water column thickness is particularly important in the southern part of the model domain because of the proximity of the critical latitude(s) for the semi-diurnal constituents (Ramming and Kowalik, 1978). The critical latitude for a given constituent is defined as the latitude where the inertial frequency is equal to the tidal frequency for that constituent. Higher than the critical latitude the amplitude of the tide becomes strongly depth-dependent. Thus, it may be possible to improve the model's fit in this area by altering the

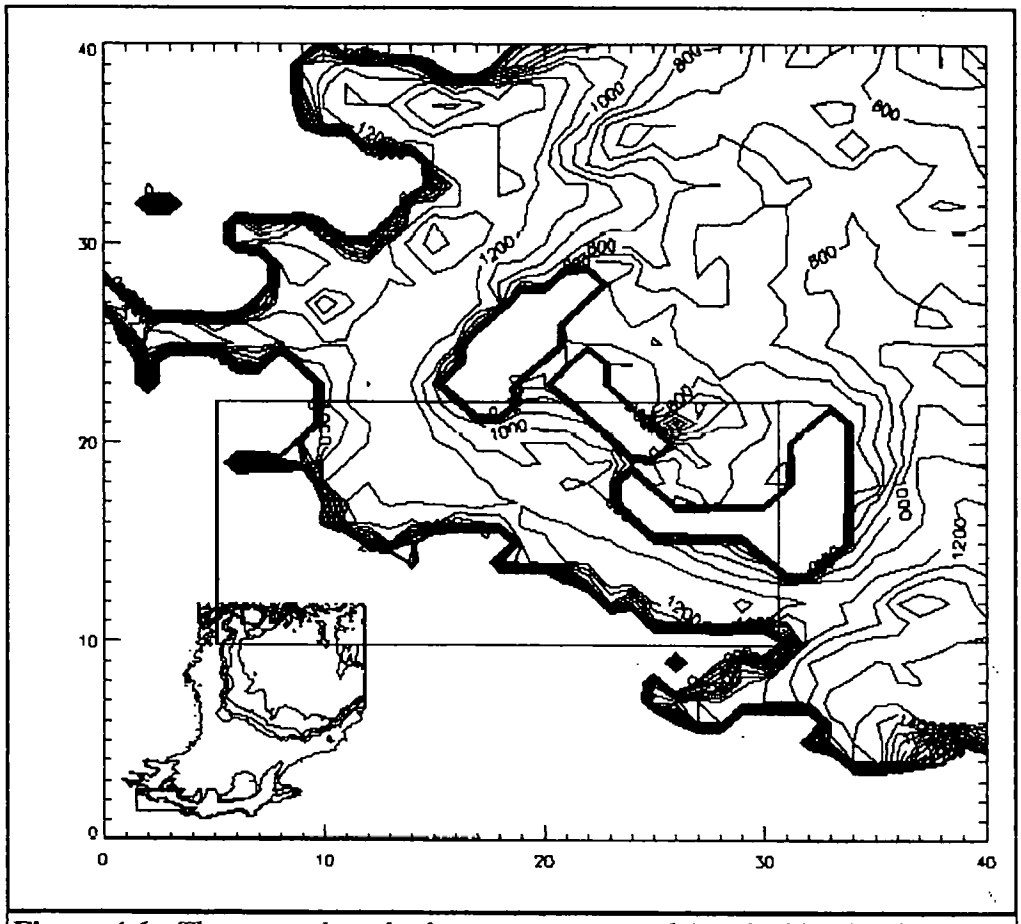

Figure 4.6: *The area where bathymetry was varied (marked by thin black line) in order to change the geometry of the sub-ice shelf cavity. Inset shows the position of this area with respect to the rest of the model domain.*

bathymetry in the model domain, in addition to gauging the effects of errors in topography upon the model's results.

Altering the geometry of the sub-ice shelf cavity

Examination of Table 3.1 and Table 3.2 indicates that between sites 16 and 13, the diurnal constituents (O1 and K1) have significantly different phase changes. In Table 3.1 (the real tidal data) the difference between O1 and K1 phases ($G_{O1} - G_{K1}$) at Site 13 is -8°, and +14° at Site 16. In Table 3.2 (the modelled data) the phase differences are +30° and +28° respectively. There are several possible reasons for this, the model not accounting for ice shelf bending, for the interaction of frictional boundary layers between the ice-

ocean and ocean-sea floor interfaces, or that the bathymetry in this area is incorrect. A similar situation can be seen between sites 7 and 8. One factor common to both areas is that the bathymetry is poorly known. A recent seismic survey (Johnson, in press) of the southern Ronne Ice Shelf indicates that maximum water column thicknesses are in the region of 2-300 m, instead of greater than 400 m which is shown on the Map of subglacial and seabed topography 1:2,000,000 Filchner-Ronne Schelfeis (1994.), i.e. the bathymetry in this region may be up to ~200 m shallower than shown on the map. Figure 4.6 shows the area within which the water column thickness was varied. The variation took the form of decreasing the bathymetry in the area by a factor of 2, 3, or 4, to completely blocking off the sub-ice shelf cavity at either end of this region. All runs were carried out using the same parameters as the run in Chapter 3.

Results from altering the geometry of the sub-ice shelf cavity.

Figure 4.7 shows the effect of the variations in the water column thickness on the r.m.s. errors between model and data at each site. The largest effect is seen at Sites 13 and 16, where an initial decrease in r.m.s. error is followed by a large increase in the error. The trend at the other sites is for a decrease in error with decreasing water column thickness. The magnitude of the decrease in error also decreases with distance from the ice shelf. Blocking the sub-ice shelf cavity had a very similar effect to decreasing the water column thickness by a factor of 4.

Conclusion from altering the geometry of the sub-ice shelf cavity

A possible explanation for the variation in decrease in error with distance from the ice shelf is that the decrease in water column thickness (and consequent increase in frictional dissipation) is again reproducing a dissipation of tidal energy that occurs in the southern parts of the ice shelf covered ocean. The most obvious mechanism which could provide this dissipation is ice shelf flexure.

Figure 4.7: Varying the geometry of the sub-ice shelf cavity

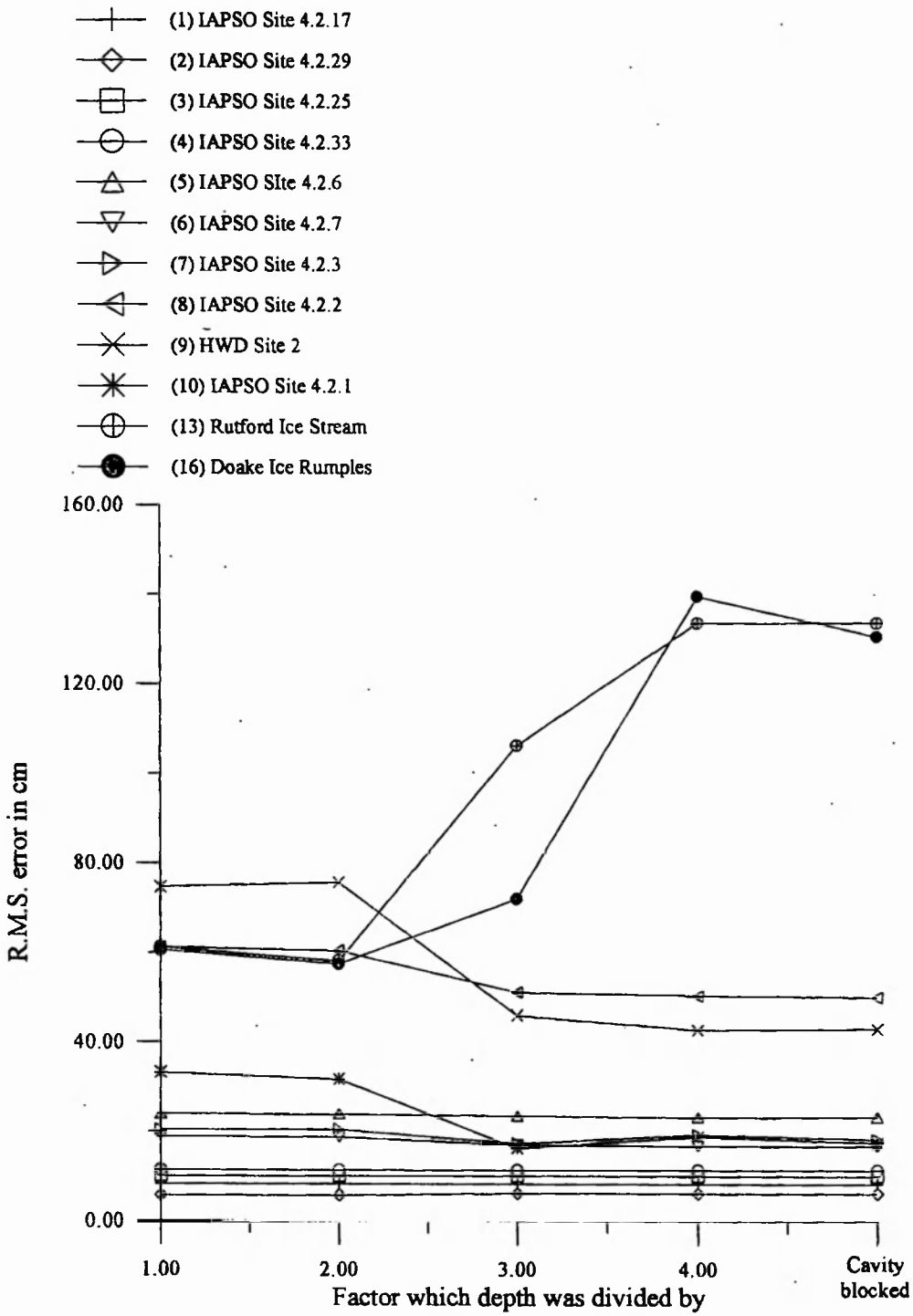

A halving of the water column thickness provides the best overall fit, though the improvement in fit is marginal and smaller than the error in the tidal data with which the model is being compared. This decrease translates to a vertical distance of 150-300 m, which is of the same order as the correction that Johnson (1995, in press) implies. The large increase in error at Sites 13 and 16 shows that the model is locally very sensitive to changes in bathymetry.

(4) Open boundary conditions:

As described in Chapter 2, the tides of the Weddell Sea are poorly known, and the data used to fit the SCH are primarily from the N.E. Atlantic (Schwiderski, 1980) whereas CR is based on satellite altimeter derived sea-surface heights from 75°N to 75°S (Cartwright & Ray, 1990) for ice-free ocean, which excludes large parts of the Weddell Sea. In particular, when the SCH model was developed (Schwiderski, 1980) there was no data available from the Atlantic sector of the Southern Ocean. Thus, both data sets have associated factors which limit their accuracy in the Weddell Sea. Variation of the open boundary conditions will be a simple comparison of the effects of using either data set.

Results from using the CR open boundary condition data

Table 4.1 shows the modelled amplitudes and phases at each site. Figure 4.8 shows the r.m.s. error in cm and as a percentage of tidal range for the comparison sites. Figure 4.9 shows the percentage difference in error using CR data compared with using SCH data (i.e. a comparison of Figures 3.6 (b) and 4.8 (b)). The overall structure of the tide was very similar to that found using SCH boundary conditions. There was a general increase in amplitude of the semi-diurnal constituents, and a decrease in amplitude of the diurnal constituents, as would be expected from comparing the two data sets (Figure 2.3). Figure 4.9 shows that while the CR boundary conditions provide a

Table 4.1: Modelled amplitude and phase data using CR open boundary data

Site	O1		K1		M2		S2	
	H(cm)	G(°)	H (cm)	G(°)	H (cm)	G(°)	H (cm)	G(°)
1	19	53	22	92	48	275	25	292
2	20	54	23	90	43	278	20	309
3	21	54	25	89	38	278	16	327
4	38	54	24	98	36	275	16	336
5	22	353	15	15	33	209	26	220
6	24	355	15	21	50	213	35	228
7	25	350	17	29	58	241	39	255
8	31	350	18	32	55	242	37	256
9	35	40	21	85	54	86	28	107
10	25	12	15	52	66	301	40	311
11	28	11	17	55	61	341	34	351
12	28	25	18	69	48	15	25	27
13	28	38	18	83	93	43	50	61
14	28	38	18	83	93	43	50	61
15	27	34	17	78	82	30	44	47
16	31	33	19	78	117	33	64	50

Figure 4.8 (a): Variation in r.m.s. error with latitude when using CR open boundary data

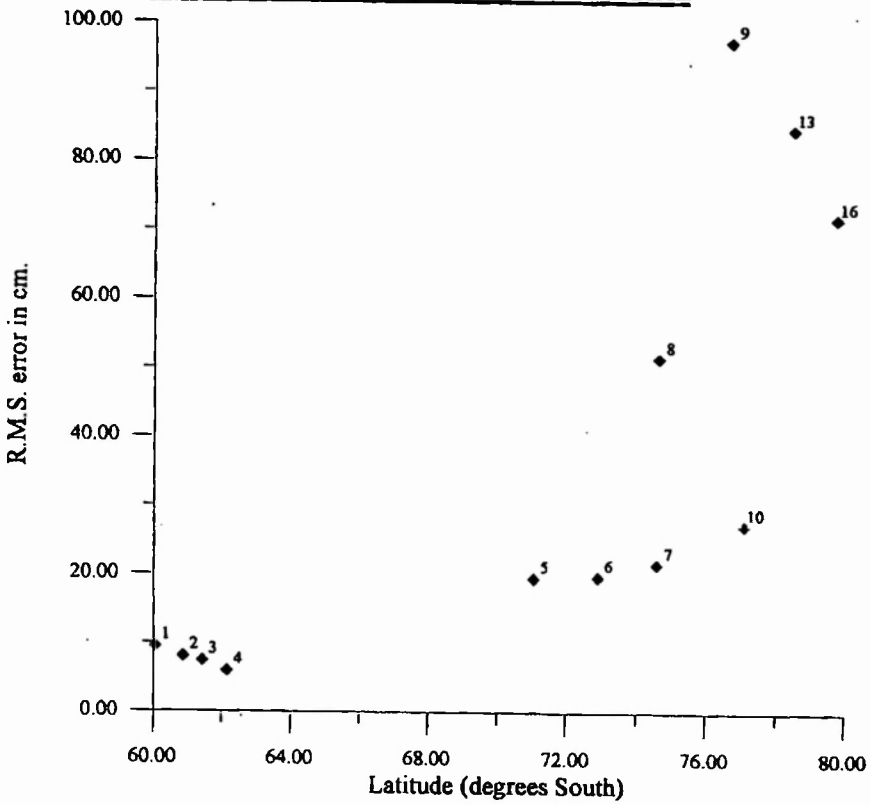

Figure 4.8 (b): Variation in percentile error with latitude using CR open boundary data

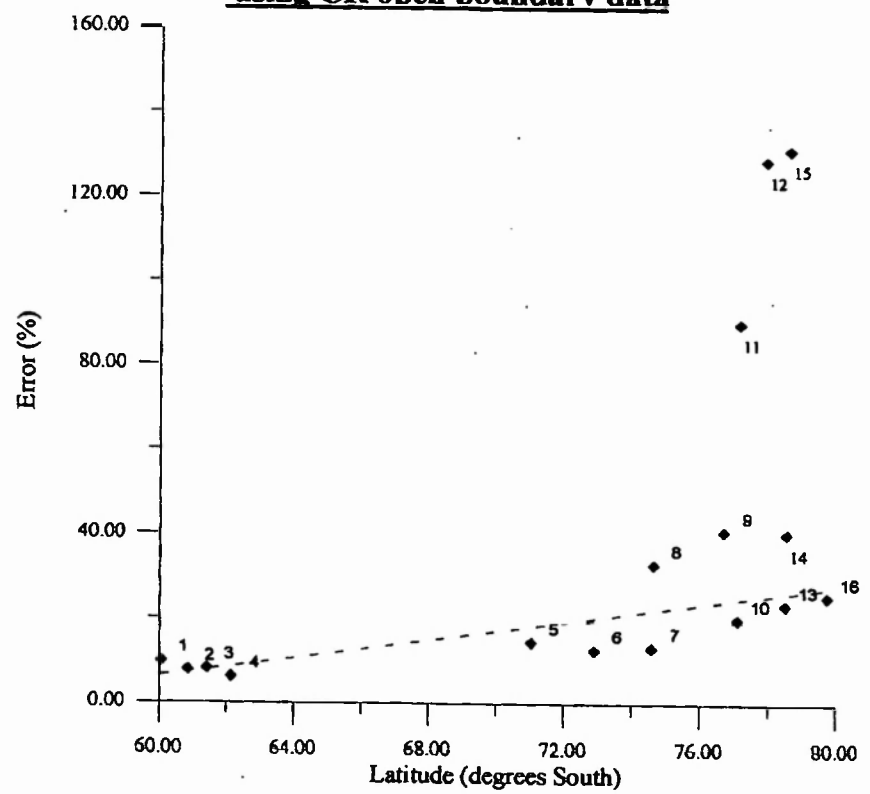

Figure 4.9: Difference (in %) between SCH & CR % error, against latitude.

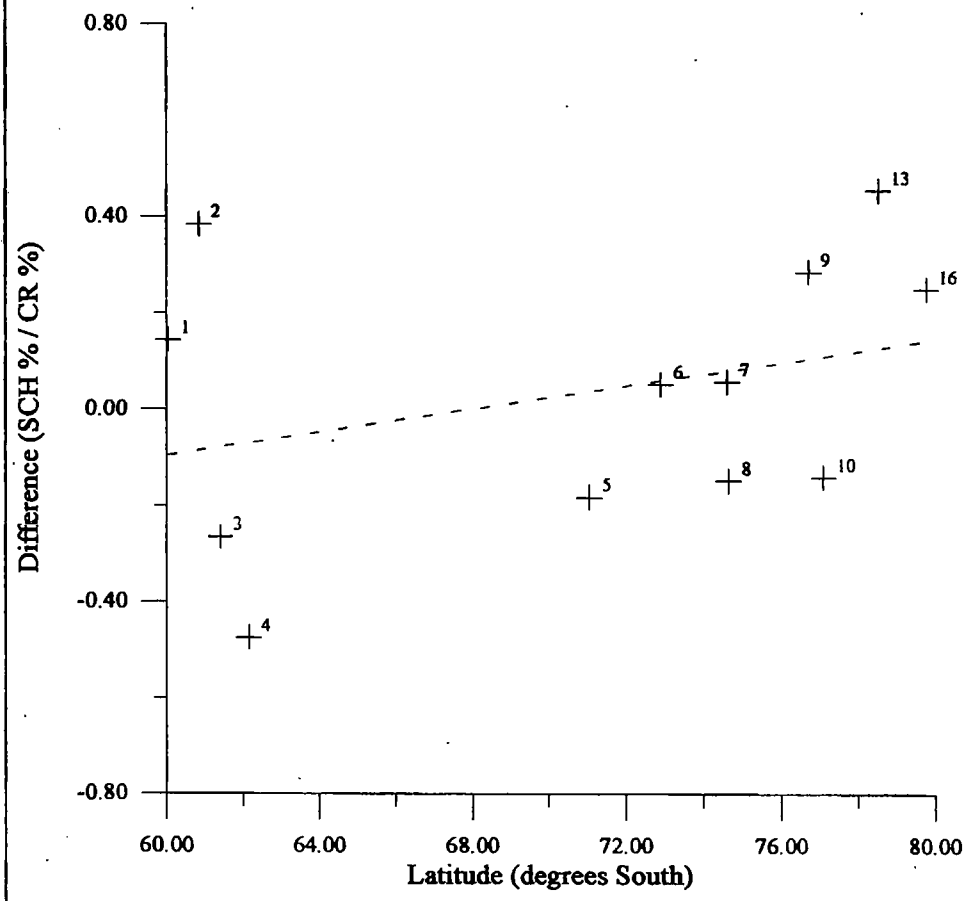

slightly better fit than SCH boundary conditions at the open boundary, this deteriorates to a slightly worse fit with increasing latitude.

Conclusion from changing open boundary condition

Overall, the results from using CR boundary data are very similar to the SCH data. The quality of fit is better than SCH at the open boundary, but is worse well away from the open boundary. In particular, the r.m.s. errors are markedly worse at Sites 9, 13 and 16. This is likely to be a result of the way the amplitudes of the CR open boundary data varies at the southern part of the open boundary (Figure 2.2), which may in turn be due to the presence of sea-ice reducing data coverage for the Weddell Sea. The conclusion is that the SCH data set provides better boundary conditions for the current model. If

the model physics were changed to improve the model's fit in the southern part of the Weddell Sea, then it is possible that CR data would provide a better fit.

CONCLUSION

It is apparent from sites 1 to 7 that the basic Flather model is insensitive to small (physically reasonable) changes in the parameters of friction and eddy viscosity. This suggests that the errors between the model and data are purely dependent on the physics contained within the model and the boundary conditions.

Changing the open boundary condition has a small effect on the overall model results, and both of the available data sets generally achieve r.m.s. errors between the model and data that are within the level required for the ESAMCA project. The poorer fit achieved at the Sites 9, 13 and 16 when using CR open boundary data indicates that SCH open boundary condition data results in a better representation of the tide in the vicinity of the ice shelf, with the present model.

For the sites on or near the ice shelf, the situation is more complex. The difference between model and data varies between sites as well as for different values of the friction coefficient, suggesting that there is some fundamental physics missing from the model. In order to fit the data, it appears that the model needs to dissipate energy near to the grounding lines. An obvious omission from the model is the effect of ice shelf bending, where the ice shelf is flexing between immobile grounded ice and freely-responding ice shelf (Williams & Robinson, 1980, 1979). Vaughan (1995) has stated that the mechanism by which ice shelves bend appears to be elastic, and therefore no energy can be dissipated within the ice shelf. MacAyeal (1979, Appendix A) showed that ice shelf flexure is important for the dynamics of a wave travelling through an ice shelf/shallow water system where the ice shelf thickness is much greater than the water column thickness. This condition is primarily (but not exclusively) met around the coast/grounding line, where the $z \approx 0$ boundary condition provides relatively (to the rest of the ice shelf covered area) sharp gradients of water column thickness and sea surface

height. The effect in the region close to the grounding line is that the ice - water interface exerts a pressure upon the underlying water column proportionate to the difference between the ice shelf motion and the sea surface motion were the ice shelf not present (Vaughan, 1995). Energy is dissipated by the work done against this pressure within the water column, and this will have the effect of lagging/damping the tidal wave.

It is also apparent from the model that though the model water column thickness (bathymetry and ice shelf thickness) may be incorrect in the very southern part of the ice shelf, simplistic attempts to correct this (by reducing water column thickness) only improve the model's fit slightly. This supports the view that the poorer fit that the model obtains under the ice shelf is due to incomplete parameterisation of the physical processes occurring underneath the ice shelf, given the accuracy achieved by the Flather model when applied to other parts of the world (Flather, 1994, 1988, 1987).

Chapter 5:

Effects upon the general oceanography of the area

INTRODUCTION

In the previous chapters I have shown that the model is able to reproduce the tides in the Weddell Sea with a reasonable degree of accuracy, and investigated the effect upon the model results of varying different parameters. I shall now go on to investigate what the model can indicate about the general oceanography of the area, in particular the conditions upon the continental shelf and beneath the ice shelves.

There are several ways in which the tides affect the water masses found in the Weddell Sea, of which the most important are horizontal advection and vertical mixing. Tides cause horizontal advection in two ways, by periodic motions and by residual currents generated by the interactions of the periodic tidal currents with variations in bathymetry. Vertical mixing can be caused by internal tides and by the generation of turbulence at the sea-floor and at the base of the ice shelf. In this chapter I will look at the periodic and residual currents generated by the "standard" model run (c.f. Chapter 3) and also attempt to gauge the generation of turbulence at the frictional interfaces by examining the amount of energy being dissipated at these interfaces.

THE PRESENT STATE OF KNOWLEDGE

Data on the oceanography of the Weddell Sea is limited to the results of various cruises (Fahrbach, 1994; Carmack and Foster, 1977; Seabrooke et al,

1971; Foldvik et al, 1984) which cover the whole Weddell Sea, and long- term current meter moorings in a few locations (Middleton and Foster, 1977; Gammelsrød and Slotsvik, 1981; Foldvik et al, 1985). Foldvik et al (1990) describe the tides of the southern Weddell Sea primarily using current meter data from the continental shelf break and from the ice front. Middleton et al (1987, 1982) used the current meter data from the continental shelf break to show the presence of continental shelf waves at diurnal and longer periods.

To summarise the current state of knowledge (which is not clear about all processes occurring within the region , or even of the relative importance of all the water masses), the central (i.e. deep ocean) Weddell Sea is dominated by the clockwise circulation of a relatively warm, salty water mass which extends from the near surface to near to the sea floor. Also existing in this region are Weddell Sea Bottom Water and Antarctic Bottom Water which (as their name implies) are found near to the sea floor because of their (respectively) increasingly low temperatures and consequently increasing densities. As mentioned in Chapter 1, Antarctic Bottom Water is a globally important water mass whose main source is found in the Weddell Sea (Foldvik and Gammelsrød, 1988). Antarctic Bottom Water is formed by the mixture of Weddell Deep Water and water masses from the continental shelf. There are four different water masses on the continental shelf. Winter Water is a water mass near freezing point with salinities lower than WDW (34.36 - 34.52 ‰) found near to the surface over most of the Weddell Sea, and is formed in winter by stratification of the water column and modified by heating and melting in summer (Foster and Carmack, 1976). The mixture of WW and WDW is described as Modified Weddell Deep Water, and this water mass encroaches onto the continental shelf in places. Eastern Shelf Water is a similarly cold, but slightly fresher water mass than WW (Carmack, 1977), while Western Shelf Water is also near the freezing point, but has a salinity of greater than 34.70. ESW is found on the eastern continental shelf, and WSW is found on the western continental shelf, with the highest salinities being found in the Ronne Depression just in front of the Ronne Ice Front The last

water mass on the continental shelf is Ice Shelf Water. ISW is formed by the mixture of WSW with fresh water melted from the underside of the Filchner-Ronne Ice Shelf. The depth dependence of the freezing point, and the depth of the base of the ice shelves results in ISW being potentially super cooled (i.e. below surface freezing point for a given salinity). There are two possible routes whereby the water masses on the continental shelf may act as precursors for AABW. The first is the mixture of MWDW (the admixture of WW/ESW with WDW) with WSW and WDW at the continental shelf break, to form WSBW, which is modified by further mixing with WDW to form ABW. The other possibility is direct mixing of ISW with WDW to form WSBW or ABW. Because of a lack of evidence for the transport of unmodified ISW beyond the continental shelf break, the first mechanism is generally considered to be more important.

MIXING

One of the most important ways in which the tides may affect the structure and composition of the water masses on the continental shelf is by mixing. Tidally generated mixing can be separated into horizontal and vertical components. The horizontal component is caused by the advection of water masses out of their area of formation and into contact with other water masses. This can result from either periodic or residual tidal currents. Because the Flather model is depth-averaged over the water column, and because of the depth-dependence of tidal currents south of the critical latitude, the currents produced from the model cannot be directly compared to measured currents, without making assumptions about the eddy viscosity coefficient (Nøst, 1993). Since there are no current profiles for the area, other than those mentioned in Middleton et al (1982) it is not possible to make any reasonable assumptions about the eddy viscosity profile, other than the basic assumption in the model, that the eddy viscosity is constant. Nevertheless, by looking at the tidal currents in the model, we can gain an idea of the magnitude of horizontal advection which may be caused by the tides.

Vertical mixing results from by the generation of turbulence at the sea floor and ice shelf base, by the flow of water over them. The diffusion of this turbulence away from the sea floor/ice shelf base mixes the water column. Turbulence is also generated throughout the water column by eddy viscosity, but this is of a much smaller magnitude than the turbulence generated at sea-floor and ice shelf base. Since the Flather model is depth-averaged it is not possible to study the actual generation of turbulence (without making the assumptions mentioned above). However, by looking at the amount of energy dissipated by the frictional terms in equations 2 and 3 (Chapter 2, page 8), the average power available to cause mixing can be found.

The amount of energy dissipated by mixing associated with bottom friction is given by equation 4 (Chapter 4, page 47). The energy dissipated by eddy viscosity per unit volume and time is:

$$\frac{1}{T}\int(\rho.A_h.\nabla^2\,\mathbf{q}.h)dt$$

where

A_h is the eddy viscosity coefficient;

h is the water column thickness.

In both these cases, the r.m.s. energy dissipation is calculated over a period of a year (in a similar way to the sea surface height differences in Chapters 3 and 4) from the sum of the currents generated by each constituent at each instant of time:

$$Q=\frac{1}{T}\int_0^T\sqrt{(\sum_{i=0}^{n}(q_i.\cos(\omega_i t+g_i)))^2}\;dt$$

where

Q is the time average, depth-mean current;

$\mathbf{q}_i$ is the amplitude of the depth-mean current of constituent i;

g_i is the phase of constituent i;

ω_i is the frequency of constituent i.

MODELLED MIXING

Figures 5.1. (a) to (d) show plots of the current ellipses for each of the four modelled constituents. Unsurprisingly it can be seen that in the deep, central Weddell Sea peak tidal velocities are small (< 0.1 ms^{-1}), with much larger velocities being found on the continental shelf. Also as expected, it can be seen that on the continental shelf the major axes are aligned parallel to the contours of water column thickness, and that the ellipses become more circular as the water column shallows, indicating the regions where friction is playing an important role. This occurs because of the cubic relation between frictional energy and velocity (equation 4), the inverse relation between frictional energy and water column thickness (equations 2 and 3), and the inverse relation between water column thickness and velocity (equation 1). For the diurnal constituents O1 (Fig. 5.1. (a)) and K1 (Fig. 5.1. (b)) it can be seen that the direction of rotation of the current ellipses changes from clockwise to anticlockwise at the continental shelf break. It can also be seen that in this area the K1 tidal current ellipses are larger than the O1 and that the diurnal currents are larger than the semi-diurnal currents though the semi-diurnal tidal heights are larger than the diurnal tidal heights. A similar pattern of amplification of diurnal (J1, P1 and K1) currents relative to O1, and diurnal currents larger than semi-diurnal was found by Middleton et al (1987, 1982) in their analysis of a series of current meters from the continental shelf break. They attributed this to the existence of barotropic shelf waves at diurnal and longer periods which caused increasing amplification of diurnal currents near to the frequency of the P1 constituent. However they also found a lack of amplification of O1 currents, which the model does not reproduce since the O1 currents are also greater than the semi-diurnal currents. No physical basis has been found for this lack of amplification of O1 currents (or rather of currents below P1 frequency). Another point of interest is the region of low currents north of Berkner Island. This area was found (Foldvik et al, 1985) to be an area where HSSW is formed. Low currents indicate less energy available for the generation of polynyas in the pack ice, which would indicate an area where HSSW is less likely to be formed. However Berkner Island

(Figure 1.1) may provide an alternate means of creating coastal polynyas, by the action of katabatic winds flowing from the summit of Berkner Island. Figures 5.2 (a) shows a contour plot of energy dissipation by bottom friction which takes in to account the higher friction coefficient under the ice shelf, and Figure 5.2(b) shows a contour plot of energy dissipation by eddy viscosity. It can be seen that the areas of highest energy dissipation are where they would be expected from the current plots and the water column thickness. The results from varying the sub-ice shelf friction coefficient (Chapter 4) indicated that the model achieved the best fit with sites near to grounding lines (Sites 13 and 16) when applying a multiplier of 25 or 50 to the friction coefficient. Assuming that this reproduces the total energy dissipation by ice shelf flexure that occurs near to grounding lines, then concentrating this energy dissipation into the area of ice shelf within a few ice shelf thicknesses of the grounding line (Vaughan, 1994) would result in an increase in energy dissipation in those areas on the order 10^3. This would still leave the area of greatest energy dissipation being the shallow area of continental shelf just inland from the Ronne Ice Front. However, it is likely that the problems with the bathymetry data set (Chapter 2) make the model erroneous in these regions.

Figure 5.2 (b) shows that the distribution of energy dissipation by eddy viscosity is fairly uniform, varying by only one order of magnitude from a mean value of 6.3×10^{-2} W m^{-2}, compared with the 2.5 order of magnitude variation of frictional dissipation. This uniformity is expected because of the velocity-depth relation in eddy viscosity. The energy dissipation by eddy viscosity clearly shows a pattern of small peaks and troughs in the vicinity of the continental shelf break. These variations are presumably related to the amplification of diurnal currents described above.

Both figures show a significant peak where the eastern boundary intersects the coast. This is due to the shape of the coastline, the shallow water column at the coast and the steep offshore bathymetry gradients, which force the flow of water from the open boundary point adjacent to the coast into a predominantly

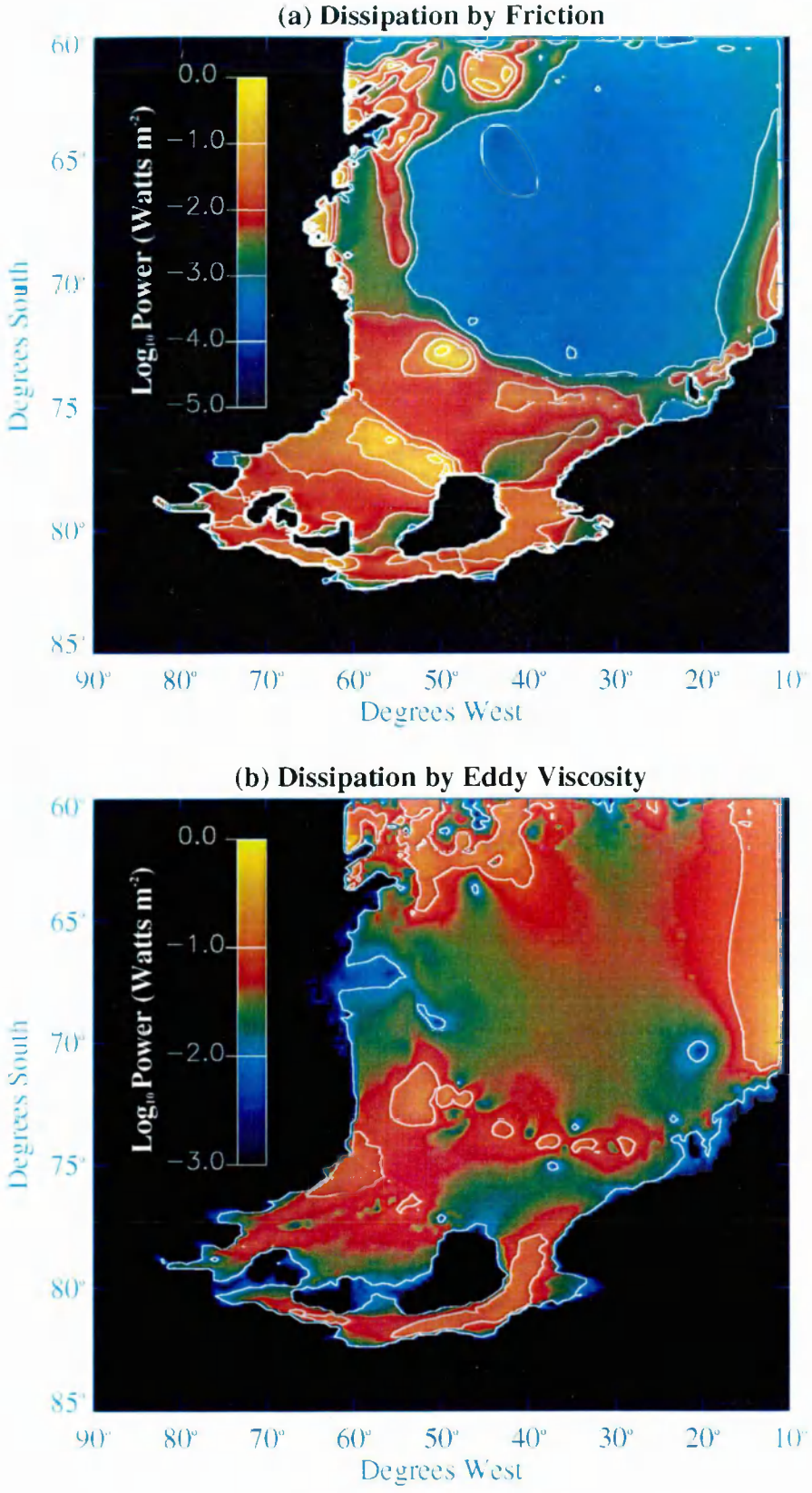

Figure 5.2: Modelled mean annual tidal energy dissipation by:

(a) Friction between ocean and sea-floor/ice shelf base

(b) Eddy Viscosity within water column.

northerly direction. As mentioned in Chapter 2, coastal bathymetries are probably erroneous, and the elevation-specified character of the open boundary prevents currents from flowing out of the model domain. Thus this feature is probably an artefact of the model and its interaction with the domain.

TIDAL RECTIFICATION

Another important way in which the tides can effect the general oceanography of the area is the generation of residual currents by tidal rectification (MacAyeal, 1979; Magnell et al, 1980; Loder, 1980). The residual currents are produced directly from the "least squares" harmonic analysis. A vector plot of the currents is shown in Figure 5.3. It can be seen that the largest residuals are generated where large changes in topography coincide with large periodic currents. Thus the largest residuals are seen on the continental shelf break, and at the edge of the Filchner Depression between Berkner Island and Henry Ice Rise. In general the pattern of tidal residual currents bears little relation to the general circulation of the area (Fahrbach et al, 1994b; Carmack and Foster, 1975). However , under the ice shelf, Figure 5.3 does show many similarities to common assumptions about the sub-ice shelf currents (Nøst and Foldvik, 1994; Robin et al, 1983), such as discrete patterns of out- and inflow the Ronne Ice Front, and the circulation within the Filchner Depression. The significant difference is that there is very little communication between the Filchner and Ronne Depressions, whereas Nøst and Foldvik (1994) showed that there must be a flow of water between the two depressions, and deduced a residence time of ~7 years for water flowing from the Ronne Ice Front over Ronne Depression, to the Filchner Ice Front. This implies a mean velocity of ~0.005 ms^{-1}, which is significantly greater than the tidal residual velocities in the two depressions (~0.001 - 0.002 ms^{-1}). However as the flow from Ronne to Filchner Depression is likely to be gravity driven, tidal residuals may still represent a significant contribution to the sub-ice shelf circulation.

Figure 5.3: *Residual current vectors for the standard run (Chapter 3). Grey arrows are 1/10 of the amplitude of equivalent length black arrows.*

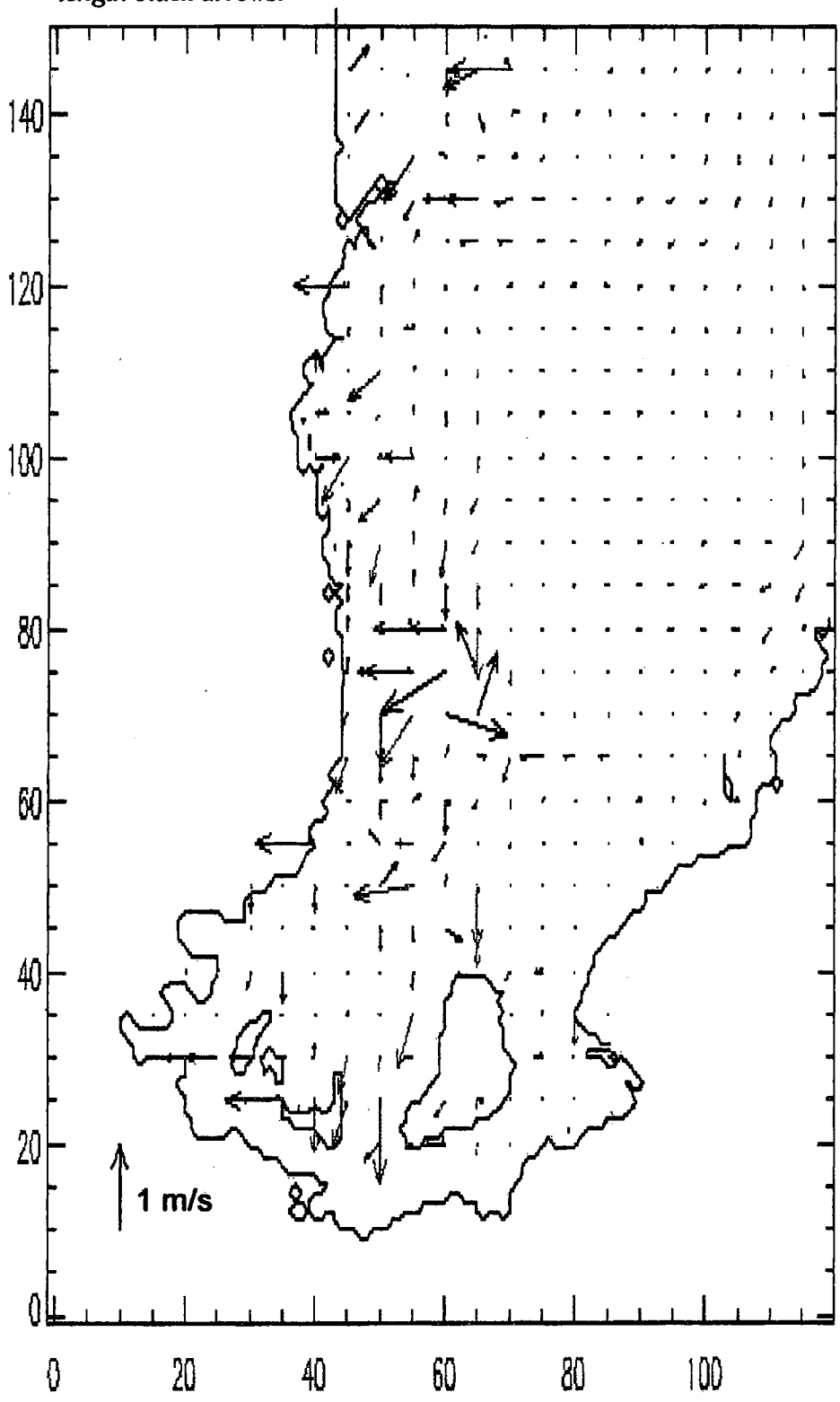

CONCLUSION

In this chapter I have looked at what the results from the tidal model can tell us about the general oceanographic conditions in the Weddell Sea. Because the model is two-dimensional, it has only been possible to study the depth-averaged periodic and residual currents and to study the way energy is dissipated within the model.

In the "open" Weddell Sea, the model partially reproduces some known features, such as the amplification of diurnal currents that occurs at the continental shelf break. In this particular case, the poorly known bathymetry and large grid size of the model prevent an accurate reproduction of the barotropic shelf waves that are found along the shelf break (Middleton et al, 1994, 1982).

For energy dissipation the model has shown the expected correlation with water column thickness. In addition the pattern of dissipation indicates that the most significant area of energy dissipation is under the Ronne Ice Front and even if dissipation by ice-shelf flexure was included, this area would still dominate dissipation. This implies that globally significant amounts of energy are not dissipated by the grounding lines of ice shelves in the Antarctic.

Summary

Chapter 1.

The Weddell Sea is a region where a globally important water mass, AABW, is produced. The Filchner and Ronne ice shelves cover the southern part of the Weddell Sea. Tides are believed to play an important role in the mechanisms which form AABW, but because of the inaccessible nature of the Weddell Sea, and in particular the southern Weddell Sea there is little tidal data available. Therefore modelling the tides should provide information about the structure of the tides, which improve understanding of the general oceanographic conditions of the area. There have been two previous attempts to model tides beneath an ice-shelf, both of which have some limitations. For this study a tidal model developed at the Proudman Oceanographic Laboratory and used operationally by the U.K. Meteorological Office was used.

Chapter 2.

The constituent equations of the model and the models structure are described. The bathymetry and ice-shelf thickness data sets which were used to form the model domain are discussed. These data sets suffer from poor data coverage in many areas covered by the model, thus possibly reducing the accuracy of the model. The model is driven by specifying the sea surface motion along the open boundary (Figure 1.1), using data taken from the Schwiderski (1980) global ocean tidal model , which is compared with Cartwright and Ray's (1990) tidal analysis of TOPEX/Poseidon satellite altimeter data.

Chapter 3.

The available tidal data for the Weddell Sea is discussed. It comprises 16

different sites, 8 of which are in the southern Weddell Sea. The method by which the model was compared to these sites is described, and then used in a comparison of a "standard" model run and the 16 sites for which there is tidal data. The model achieves good overall agreement with the data, and clearly shows an amphidrome in the semi-diurnal tidal constituents. This amphidrome was postulated by Doake (1992) using tidal data from the area of Filchner-Ronne Ice Shelf, and was also found in the Le Provost et al (1994) global tidal model, and in the Genco et al (1994) application of this model to the South Atlantic. Therefore it is reasonable to assume that this is a real feature of the tides that the model is reproducing. Differences between this model run and the data are concentrated at three sites from the Ronne Ice Shelf (Sites 11, 12, and 15). Because these sites were of short duration and provided contradictory information about the four constituents for which they had been analysed, it was decided to not use them in further studies of the model sensitivities. In addition Site 14 was not used because it was located very close to Site 13, and because the amplitudes from this site are liable to be erroneous due to the technique (tiltmeter) which was used to gather the data.

Chapter 4.

Having shown in Chapter 3 that the model can achieve a reasonable fit to the available data using some basic assumptions about the effect of the ice shelf upon the tides, the sensitivities of the model results to changes in the model parameters were examined. The model is not significantly sensitive to variations in internal parameters such as the value of the friction coefficient, in the open ocean. In the ice-shelf covered region, the model achieves best fit at different values of friction coefficient for different sites. The conclusion that higher friction is required to achieve a reasonable fit with data from sites near to the grounding line. Given that the model does not include the effect of ice shelf flexure, it would appear that large increases in the friction coefficient beneath the ice shelf go some way to replicating the effect of ice shelf flexure at sites close to the grounding line.

Varying the water column thickness in one particular region of the ice shelf, south of Korff and Henry Ice Rises, where the bathymetry data set have very

little data can improve the quality of fit the model achieves at sites in that region, with the best fit being achieved when the new water column thickness approximates to recent measurements of the bathymetry in this region. Thus it may be concluded that errors between the model and available data may largely be due to errors in the model domain, or to elements of the tidal dynamics which are not included in the model.

Chapter 5.

Tides affect the general oceanography by the generation of horizontal advection and vertical mixing. In order to gauge their importance, the magnitude and distribution of these effects within the model was studied. For both effects the area with the greatest magnitude was on the continental shelf just inshore from the ice front, and at the continental shelf break. This is a result of the effect of rapid changes in water column thickness upon the depth-averaged current. The likely magnitude of energy dissipation by ice-shelf flexure near to the grounding line is probably less than the energy dissipation near to the ice front, though this may change as ice shelf thickness changes.

Overall Conclusions

An existing tidal model has been presented and applied to a poorly studied area, the Weddell Sea. It has been shown that the inclusion of simple assumptions about the effect of the presence of ice shelves upon the tides allows the model to produce a good match with the available tidal data. Tests of the sensitivity of the model results to variations in a variety of model parameters such as friction and eddy viscosity coefficients demonstrate that the model is insensitive to small variations in these parameters. Large increases in the friction coefficient improve the model fit at two sites close to the grounding line of the ice shelves. This suggests that ice shelf flexure can be represented locally by an increase in the friction coefficient, and that the effects of ice shelf flexure are not globally important. Further results indicate that by far the most energy is dissipated around shallow areas of ice shelf covered continental shelf.

Appendix A:

Future work.

The modelling exercise presented in this thesis has reproduced the tides of the Weddell Sea. There are several possible ways of extending this modelling exercise in order to produce more detailed and more accurate models of the tides, in particular for the Filchner and Ronne Ice Shelves.

A more detailed model:

The simplest extension of the modelling would be to restrict the model domain to only covering the ice shelf covered area. Covering a smaller area would allow a smaller grid size to be used. This would be important for the ice shelf covered area because of the (apparently) localised effects of ice shelf flexure. In the present model domain, the length scales over which ice shelf flexure is important are less than the smallest grid spacing within the model. If grid size is decreased then the effects of ice shelf flexure may become important enough to be included within the model.

However a practical problem with decreasing grid size is that according to the Courant-Friedrichs-Lewy stability condition (page 16) the time step must decrease according to the square root of the decrease in grid size. For a model domain with the same number of grid points this will result in a greater length of computation time.

Better physics within the model

The main physical effect which has not been explicitly included is that of ice shelf bending. As stated in the above paragraph, a more detailed model focusing on the ice shelf covered area should at least try to include this effect because a smaller grid size will increase the number of grid points which are affected by ice shelf bending (from an apparent value of zero using the present domain). Vaughan (1995) derived equations for the effect of ice shelf flexure on the motion of the ice shelf surface in response to the tides (page 11). This equation uses the response of the ice shelf as a proportion of its motion beyond the zone of influence of ice shelf flexure. Thus a factor could be calculated for each grid node in the model domain, dependent on the ice shelf thickness and distance from grounding line which can be applied as a modifier to calculated sea surface heights within the model. Including the effect of ice shelf flexure in this way assumes that there will not be a large effect on the overall structure of the tides, i.e. that the effects of ice shelf flexure are essentially localised in extent.

Comparison with satellite altimetry

Because of the lack of tidal data in the Weddell Sea, an accurate picture of the tides will only be obtained if more data on the tides are obtained. One way of achieving this is to apply the tidal data obtained from the model to ERS-1 satellite altimeter data for the Filchner and Ronne ice shelves, to see if the tidal corrections reduce the variance between different passes of the satellite. This work is currently being undertaken as part of the ESAMCA project.

Appendix B

Corrections to the tidal data for Sites 11, 12, and 15.

Since the work in this thesis was carried out, it has come to light tha t a mistake was made (K. Makinson, pers. comm) in the analysis of the gravimeter data for Sites 11, 12, and 15 (Doake, 1992). The mistake appears to have been the omission of a minus sign in the conversion from units of gravity (milligals) to height. This resulted in the analysed tides being the inverse of the true tides, so that in Table 3.1 the phases for Sites 11, 12, and 15 are wrong by 180 degrees for all constituents. Using the correct phases, the r.m.s. error for these sites is reduced to approximately 50 cm by the corrected phases (Robinson et al, unpublished report) which is comparable with the other ice shelf sites (Sites 9, 13 and 16). Moreover, as with the other ice shelf sites, the modelled tide is in phase with the measured tide, all of the error being in the amplitude of the modelled tide. This implies that some physics of the way tides propagate through ice covered waters is missing from the model, and/or the measured amplitudes are incorrect. Because of the nature of gravimeter data it is not possible at this time to distinguish between the two possibilities.

References:

Andersen, O. B., 1994: Ocean tides in the northern North Atlantic and adjacent seas from ERS 1 altimetry, *J. Geophys. Res.*, **99**, 22557-22573.

Carmack, E. C., 1974: A quantitative characterization of water masses in the Weddell Sea during summer, *Deep-Sea Res.*, **21**, 431-442.

Carmack, E. C., and T. D. Foster, 1975: On the flow of water out of the Weddell Sea, *Deep-Sea Res.*, **22**, 711-724.

Carmack, E. C., and T. D. Foster, 1975: Circulation and distribution of water masses near Filchner Ice Shelf, *Deep-Sea Res.*, **22**, 77-90.

Cartwright, D. E., 1979: Analyses of British Antarctic Survey tidal records, *Br. Antarct. Surv. Bull.*, **49**, 167-179.

Cartwright, D. E., J. M. Huthnance, R. Spencer, and J. M. Vassie, 1980: On the St.Kilda shelf tidal regime, *Deep-Sea Res.*, **27A**, 62-70.

Cartwright, D. E., and R. D. Ray, 1990: Oceanic tides from Geosat altimetry, *J. Geophys. Res.*, **95**, 3069-3090.

Deacon, G. E. R. 1937: The hydrology of the Southern Ocean, *Discovery Rep.*, **15**, 1-24.

Dietrich, G., 1980. General Oceanography: An Introduction, Wiley-Interscience, New York.

Doake, C. S. M., 1978: Dissipation of tidal energy by Antarctic ice shelves, *Nature*, **275**, 304-305.

Doake, C. S. M., 1992: Gravimetric tidal measurements on Filchner-Ronne Ice Shelf, *Filchner Ronne Ice Shelf Programme Report No. 6*, pp. 34-39, ed Oerter, H., Alfred-Wegener Institute for Polar and Marine Research, Bremerhaven, Germany.

Fahrbach, E., G. Rohardt, M. Schröder, and V. Strass, 1994: Transport and structure of the Weddell Gyre, *Ann. Geophysicae*, **12**, 840-855.

Fahrbach, E., G. Peterson, G. Rohardt, P. Schlosser, R. Bayers, 1994: Suppression of bottom water formation in the southeastern Weddell Sea, *Deep-Sea Res.*,**41**, 389-411.

Flather, R. A., 1994: A storm surge prediction model for the Northern Bay of Bengal with application to the Cyclone Disaster in April 1991, *J.Phys.Ocean.*, **24**, 172-190.

Flather, R. A., 1988: A numerical model investigation of tides and diurnal period continental shelf waves along Vancouver Island, *J.Phys.Ocean.*, **18**, 115-139.

Flather, R. A., 1987: A tidal model of the north-east Pacific. *Atmos. Ocean.*, **25**, 22-45.

Foldvik, A., J. H. Middleton, and T. D. Foster, 1990: The tides of the southern Weddell Sea, *Deep-Sea Res.*, **37**, 1345-1362.

Foldvik, A. and T. Gammelsrød, 1988: Notes on Southern Ocean hydrography, sea-ice and bottom water formation, *Palaeogeog. Palaeoclim. Palaeoeco.*, **67**, 3-17.

Foldvik, A., T. Kvinge, and T. Tørresen, 1985b: Bottom currents near the continental shelf break in the Weddell Sea, *Ant. Res. Ser.*, **43**, 21- 34.

Foldvik, A., T. Gammelsrød, and T. Tørresen, 1985a: Circulation and water masses on the southern Weddell Sea shelf, *Antarctic Research Series*, **43**, 5-19.

Foster, T. D., and E. C. Carmack, 1976: Frontal zone mixing and Antarctic Bottom Water formation in the southern Weddell Sea, *Deep-Sea Res.*, **23**, 301-317.

Foster, T. D., A. Foldvik, and J. H. Middleton, 1987: Mixing and bottom water formation in the shelf break region of the southern Weddell Sea. *Deep-Sea Res.*, **34**, 1771-1794.

Gammelsrød, T., and N. Slotsvik, 1981: Hydrographic and Current Measurements in the southern Weddell Sea 1979/80. *Polarforschung*, **51**, 101-111.

Genco, G. L., F. Lyard, and C. Le Provost, 1994: The oceanic tides in the southern ocean, *Annales Geophysicae*, **12**, 868-886.

Gill, A. E., 1986: Atmosphere-Ocean Dynamics, Academic Press, New York.

Gill, A. E., 1973: Circulation and bottom water production in the Weddell Sea, *Deep-Sea Res.*, **20**, 111-140.

Gjevik, B., E. Nøst, and T. Straume, 1994: Model simulations of the tides in the Barents Sea, *J.Geophys.Res.*, **99(C2)**, 3337-3350.

Godin, G., 1986: Modification by an Ice cover of the tide in James Bay and Hudson Bay, *Arctic*, **39**(1,March), 65-67.

Godin, G., and F. G. Barber, 1980: Variability of the tide at some sites in the Canadian Arctic, *Arctic*, **33**(1,March), 30-37.

Godin, G., and A. Martinez, 1994: Numerical experiments to investigate the effects of quadratic friction on the propagation of tides in a channel, *Cont.Shelf.Res.*, **14**(7/8), 723-748.

Holdsworth, G., 1977: Tidal interaction with ice shelves, *Annal. de. Geoph.*, **33**, 133-146.

Holdsworth, G., 1969: Flexure of a floating ice tongue. *J. Glaciol.*, **8**, 385-397.

Johnson, M. R., 1995: Spot depth seismics over Southern and Western Ronne Ice Shelf, *Filchner Ronne Ice Shelf Programme Report No. 9*, in press.

Kowalik, Z., 1994: Modelling of topographically amplified diurnal tides in the Nordic Seas, *J.Phys.Ocean.*, **24**, 1717-1731.

Kowalik, Z., and J. B. Matthews, 1982: The M2 tide in the Beaufort and Chukchi Seas, *J.Phys.Ocean.*, **12**, 743-745.

LaBrecque, J. L. and M. E. Ghidella, 1992: Estimates of bathymetry, depth to magnetic basement and sediment thickness for the western Weddell Basin, *Antarctic Journal*, **27**, No. 5, 68-70.

Le Provost, C., M. L. Genco, F. Lyard, P. Vincent, and P. Canceil, 1994: Spectroscopy of the worlds ocean tides from a finite element hydrodynamic model, J.Geophys.Res..

Loder, J. W., 1980: Topographic rectification of tidal currents on the sides of Georges Bank, *J.Phys.Ocean.*, **10**, 1399-1416.

Lutjeharms, J. R. E., C. C. Stavropoulis, and K. P. Koltermann, 1985: Tidal measurements along the Antarctic coastline, in *Oceanology of the Antarctic Continental Shelf, Antarctic Res. Ser.*, vol. **43**, edited by S. S. Jacobs, pp. 273-289, AGU, Washington, D. C.

MacAyeal, D. R., 1984a: Thermohaline circulation below the Ross Ice Shelf: a consequence of tidally induced vertical mixing and basal melting, *J. Geophys. Res.*, **89**, 597-606.

MacAyeal, D. R., 1984b: Numerical simulation of Ross Seas tides, *J. Geophys. Res.*, **89**, 607-615.

MacAyeal , D. R., 1979: Rectified tidal currents and tidal-mixing fronts: controls on the Ross Ice Shelf flow and mass-balance, Ph.D. thesis, Princeton Univ., Princeton, N.J., U.S.A.

Magnell, B. A., S. L. Speigel, R. I. Scarlet, and J. B. Andrews, 1980: The relationship of tidal and low-frequency currents on the north slope of Georges Bank, *J.Phys.Ocean.*, **10**, 1200-1212.

Mantyla & Reid, 1983: Abyssal characteristics of the world ocean's waters. *Deep-Sea Res.*, **30**, 805-833.

Map of subglacial and seabed topography 1:2,000,000 Filchner-Ronne-Schelfeis / Weddell Sea, Antarktis. Institut für Angewandte Geodäsie, Frankfurt am Main, 1994.

Middleton, J. H., and T. D. Foster, 1977: Tidal currents in the central Weddell Sea, *Deep-Sea Res.*, **24**, 1195-1202.

Middleton, J. H., T. D. Foster, and A. Foldvik, 1987: Diurnal shelf waves in the Southern Weddell Sea, *J. Phys. Oceanog.*, **17**, 784-791.

Middleton, J. H., T. D. Foster, and A. Foldvik, 1982: Low frequency currents in the southern Weddell Sea, *J.Phys.Ocean.*, **12**, 618-634.

Munk, W. H., and D. E. Cartwright, 1966: Tidal spectroscopy and prediction, *Phil. Trans. Roy. Soc. Lond. A*, **259**, 533-581.

Murty, T. S., and R. J. Polavarapu, 1978: Influence of an ice layer in the propagation of long waves, *Mar. Geod.*, **2**(2), 99-125.

National Geophysical Data Center, 1988: ETOPO-5 bathymetry/topographic data, *Data Announc.*, 88-MGG-02, Natl. Oceanic and Atmos. Admin., U.S. Dep. Commer., Boulder, Colorado.

Nicholls, K.W., and A. Jenkins, 1993: Temperature and Salinity beneath Ronne Ice Shelf, Antarctica, *J.Geophys.Res.*, **98**(C12), 22553-22568.

Nicholls, K. W., K. Makinson, and A. Robinson, 1991: Ocean circulation beneath the Ronne ice shelf, *Nature*, **354**, 221-223

Nøst, E., 1993: Calculating tidal current profiles from vertically integrated models near the critical latitude in the Barents Sea, *J. Geophys. Res.*, **99**, 7885-7901.

Nøst, O. A., and A. Foldvik, 1994: A model of ice shelf-ocean interaction with application to the Filchner-Ronne and Ross ice shelves, *J. Geophys. Res.*, **99**, 14243-14254.

Potter, J. R., and J. G. Paren, 1985: Interaction between ice shelf and ocean in George VI Sound, Antarctica, *Ant. Res. Ser.*, **43**, 35-58.

Pedley, M., J. G. Paren, and J. R. Potter, 1986: The tidal spectrum underneath Antarctic Ice Shelves, *J.Geophys.Res.*, **91**(C11), 13001-13009.

Pond, S., and G. L. Pickard, 1983: Introduction to Dynamical Physical Oceanography, Pergamon Press, Oxford.

Pratt, J. G. D., 1956: The tide at Shackleton, *Nature*, **182**, 1394.

Proctor, R. and R. A. Flather, 1983: Routine storm surge forecasting using numerical models: Procedures and computer programs for use on the CDC Cyber 205E at the British Meteorological Office. Institute of Ocean Sciences, Rep. No. 167, 171 pp.

Ramming, H. G., and Z. Kowalik, 1978: Numerical Modelling of Marine Hydrodynamics, Applications to Dynamic Physical Processes, *Oceanogr. Ser.*, vol. 26, Elsevier/North Holland, New York.

Robin, G. de Q., C. S. M. Doake, H. Kohnen, R. D. Crabtree, S. R. Jordan, and D. Möller, 1983: Regime of the Filchner-Ronne ice shelves, Antarctica, *Nature*, **302**, 582-586.

Robinson, A., K. Makinson, and K. Nicholls, 1994: The oceanic environment beneath the north-west Ronne Ice Shelf, Antarctica, *Ann. Glacio.*, **20**, 386-390.

Scheduikat, M., and D. J. Olbers, 1990: An one-dimensional mixed layer model beneath the Ross Ice Shelf with tidally induced vertical mixing, *Ant. Sci.*, **2**(1), 29-42.

Schwiderski, E. W., 1980: On charting global ocean tides, *Rev. Geophys. Space Phys.*, **18**, 243-268.

Seabrooke, J. M., G. L. Hufford, and R. B. Elder, 1971: Formation of Antarctic Bottom Water in the Weddell Sea, *J. Geophys. Res.*, **76**, 2164-2178.

Sea-Ice Climatic Atlas: Volume 1 Antarctic, 1985, Naval Oceanography Command Detachment, Asheville.

Sievers, J., C. S. M. Doake, J. Ihde, D. R. Mantripp, V. S. Pozdeev, B. Ritter, H. W. Schenke, F. Thyssen, D. G. Vaughan, 1994: Validating and improving elevation data of a satellite image map of Filchner-Ronne Ice Shelf, Antarctica, with results from ERS-1, *Ann. Glacio.*, **20**, 347-352.

Smith, A.M., 1991: The use of tiltmeters to study the dynamics of Antarctic ice-shelf grounding lines, *J. Glaciol.*, **37**, 51-58.

Smith, W. H. F., 1995: On the accuracy of digital bathymetry data, *J.Geophys.Res.*, **98** (B6), 9591-9603.

Smithson, M. J., *ed.*, 1992: *IAPSO Pulblication Scientifique No.35*, Pelagic Tidal Constants 3. International Association for the Physical Sciences of the Oceans of the International Union of Geodesy and Geophysics.

Stephenson, S. N., 1986: Glacier flexure and the position of grounding lines: measurements by tiltmeter on Rutford Ice Stream, Antarctica, *Ann. Glacio.*, **5**, 165-169.

Thyssen, F., A. Bombosch and H. Sandhäger, 1993: Elevation, ice thickness and structure mark maps of the central part of the Filchner-Ronne Ice Shelf. *Polarforschung*, **62** (1), 17-26.

Van Wyckhouse, R., 1973: SYNBAPS, *Tech. Rep. TR-233*, U.S. Nat'l Oceanogr. Off., Stennis Space Center, Miss.

Vaughan, D. G., 1995: Tidal Flexure at Ice Shelf Margins, *J. Geophys. Res.*, **100**, 6213-6224.

Visser, A. W., 1994: On Tidal Rectification and Geostrophic Degeneracy, *J.Phys.Ocean.*, **24**, 2196-2200.

Williams, R. T., and E. S. Robinson, 1980: The Ocean Tide in the Southern Ross sea, *J.Geophys.Res.*, **85**(C11), 6689-6696.

Williams, R. T., and E. S. Robinson, 1979: Ocean tide and waves beneath the Ross Ice Shelf, Antarctica, *Science*, **203**(2 Feb), 443-445.